iScience

CellPress

Article

Anisotropic Singlet Fission in Single Crystalline Hexacene

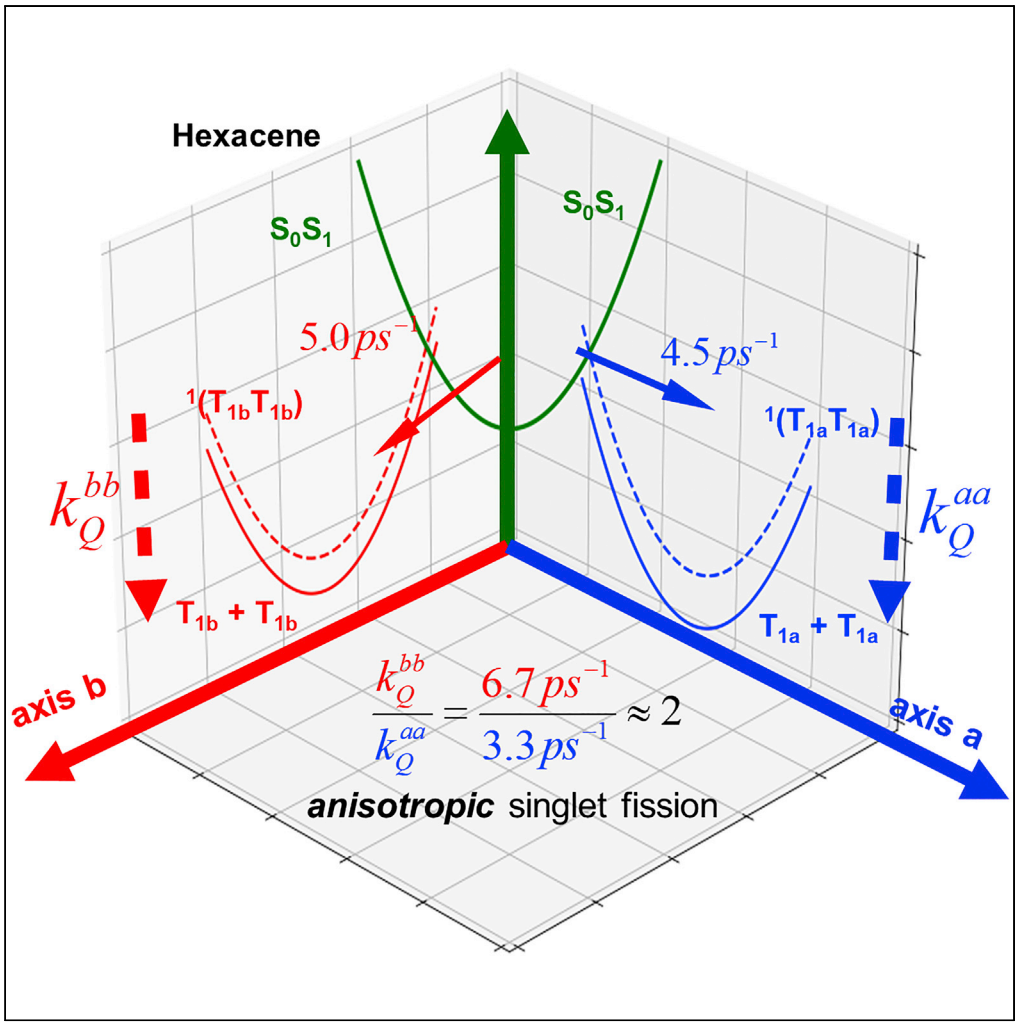

Dezheng Sun, Gang-Hua Deng, Bolei Xu, ..., Gugang Chen, Hanning Chen, Yi Rao

gchen@honda-ri.com (G.C.)
chenhanning@email.gwu.edu (H.C.)
yi.rao@usu.edu (Y.R.)

HIGHLIGHTS

Remarkable anisotropy of the overall singlet fission along different crystal axes

The correlated triplet pair emerges on the same timescale along both crystal axes

The quantum decoherence is predominantly driven by electron-phonon coupling

The anisotropic decoherence is due to the directional difference of its energy loss

Sun et al., iScience 19, 1079–1089
September 27, 2019
https://doi.org/10.1016/j.isci.2019.08.053

iScience

CellPress

Article

Anisotropic Singlet Fission in Single Crystalline Hexacene

Dezheng Sun,[2,7] Gang-Hua Deng,[1,7] Bolei Xu,[3,7] Enshi Xu,[4,7] Xia Li,[1] Yajing Wu,[3] Yuqin Qian,[1] Yu Zhong,[5] Colin Nuckolls,[5] Avetik R. Harutyunyan,[6] Hai-Lung Dai,[3] Gugang Chen,[6,*] Hanning Chen,[4,*] and Yi Rao[1,8,*]

SUMMARY

Singlet fission is known to improve solar energy utilization by circumventing the Shockley-Queisser limit. The two essential steps of singlet fission are the formation of a correlated triplet pair and its subsequent quantum decoherence. However, the mechanisms of the triplet pair formation and decoherence still remain elusive. Here we examined both essential steps in single crystalline hexacene and discovered remarkable anisotropy of the overall singlet fission rate along different crystal axes. Since the triplet pair formation emerges on the same timescale along both crystal axes, the quantum decoherence is likely responsible for the directional anisotropy. The distinct quantum decoherence rates are ascribed to the notable difference on their associated energy loss according to the Redfield quantum dissipation theory. Our hybrid experimental/theoretical framework will not only further our understanding of singlet fission, but also shed light on the systematic design of new materials for the third-generation solar cells.

INTRODUCTION

Singlet fission has recently attracted extensive attention from both experimentalists (Busby et al., 2015; Chan et al., 2011, 2012; Congreve et al., 2013; Musser et al., 2015; Walker et al., 2013) and theoreticians (Berkelbach et al., 2013a, 2013b, 2014; Tiago et al., 2003; Yost et al., 2014; Zimmerman et al., 2010; Zirzlmeier et al., 2015), since it has the potential to circumvent the Shockley-Queisser limit for solar energy utilization. Many materials have exhibited singlet fission, and they range from small molecules to polymers, and from isolated molecules, thin films, to polycrystalline materials (Burdett et al., 2010; Busby et al., 2014, 2015; Cook et al., 2016; Johnson et al., 2010; Jundt et al., 1995; Katoh et al., 1997; Marciniak et al., 2009; Michl et al., 2007; Najafov et al., 2010; Pensack et al., 2016; Schwob and Williams, 1972; Takeda et al., 1996; Tayebjee et al., 2013; Walker et al., 2013; Watanabe et al., 2006; Wen et al., 2013; Wilson et al., 2011; Zenz et al., 1999). Singlet fission is a spin-conserving process, in which a photo-generated singlet exciton is converted into two individual triplet excitons (Smith and Michl, 2010). This unique photophysical phenomenon is usually considered to proceed in two steps, namely, the formation of a correlated triplet pair, $^1(T_1T_1)$, and its subsequent quantum decoherence to engender a decoupled triplet dimer, T_1+T_1. A generic model often employed to describe the mechanism of singlet fission is given by (Merrifield et al., 1969):

$$S_0 + S_1 \xrightarrow{k_F} {}^1(T_1T_1) \xrightarrow{k_Q} T_1 + T_1 \qquad \text{(Equation 1)}$$

where S_0 is a ground state, S_1 is a singlet excited state, and k_F and k_Q denote the rate constants for the formation of $^1(T_1T_1)$ and its quantum decoherence, respectively. Despite recent tremendous efforts, the mechanisms of these two constituent steps of singlet fission (Bakulin et al., 2016; Chan et al., 2011, 2012; Miyata et al., 2017; Musser et al., 2015; Stern et al., 2017) are still not well understood.

Previous studies were primarily focused on the first step (Berkelbach et al., 2013b; Chan et al., 2013; Monahan and Zhu, 2015; Schwerin et al., 2010; Smith and Michl, 2010; Yost et al., 2014; Zimmerman et al., 2010, 2011) and have invoked three mechanisms so far to rationalize the formation of $^1(T_1T_1)$. They are the direct mechanism (Zimmerman et al., 2010, 2011, 2013), the charge-transfer (CT)-mediated mechanism (Beljonne et al., 2013; Busby et al., 2015; Chan et al., 2013; Monahan and Zhu, 2015; Smith and Michl, 2010), and the sequential mechanism (Berkelbach et al., 2013b; Nakano et al., 2016). On the other hand, the quantum decoherence of $^1(T_1T_1)$ is rarely explored, particularly from the theoretical perspective (Casanova, 2018). As a matter of fact, quantum decoherence plays a key role in singlet fission by decoupling $^1(T_1T_1)$ through vibronic coupling. Therefore, a rapid decoherence of correlated $^1(T_1T_1)$ is highly desired for an efficient production of decoupled T_1+T_1, the final product of singlet fission. Otherwise, the reverse of the singlet fission

[1]Department of Chemistry and Biochemistry, Utah State University, Logan, UT 84322, USA

[2]Department of Physics, Columbia University, New York, NY 10027, USA

[3]Department of Chemistry, Temple University, Philadelphia, PA 19122, USA

[4]Department of Chemistry, George Washington University, Washington, DC 20052, USA

[5]Department of Chemistry, Columbia University, New York, NY 10027, USA

[6]Honda Research Institute USA, Inc., San Jose, CA 95134, USA

[7]These authors contributed equally

[8]Lead Contact

*Correspondence: gchen@honda-ri.com (G.C.), chenhanning@email.gwu.edu (H.C.), yi.rao@usu.edu (Y.R.)

https://doi.org/10.1016/j.isci.2019.08.053

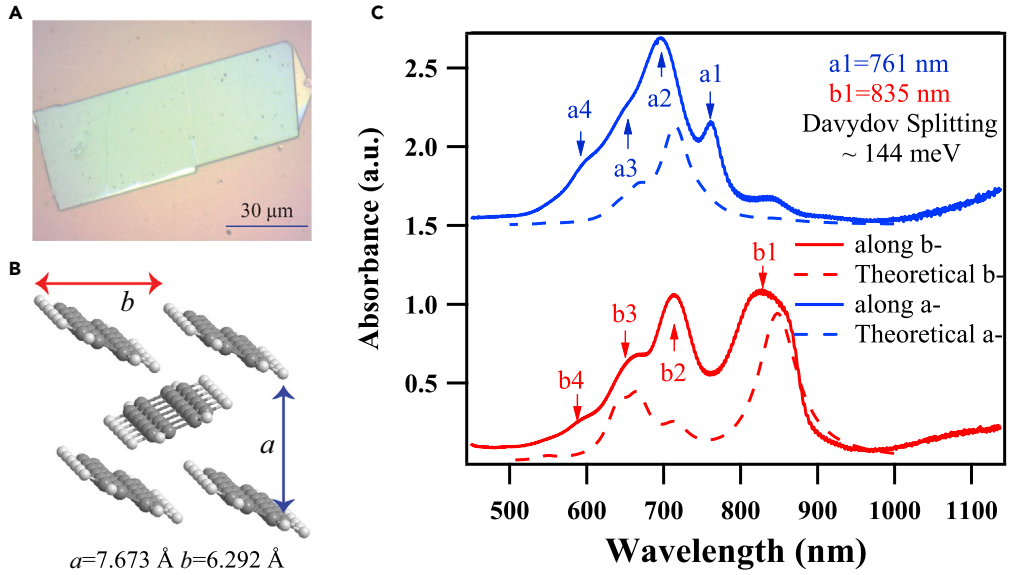

Figure 1. Polarized Linear Absorption Spectra of Single Crystalline Hexacene

(A) Optical image of one of hexacene single crystals in our experiments.

(B) The schematic of a unit cell of hexacene single crystal.

(C) Polarization resolved linear absorption spectra in the ***a***-***b*** plane of hexacene single crystals along the ***a*** (upper) and ***b*** (lower) axes. The dotted curves are the theoretical results. The lowest transition along the ***a*** axis is located at 761 nm, whereas the lowest transition along the ***b*** axis is located at 835 nm. The singlet Davydov splitting exhibits a large value of 144 meV in hexacene single crystals.

could be mediated by fusion of two triplets via triplet-triplet annihilation (Yong et al., 2017), thereby decreasing the photon-to-exciton conversion efficiency. The fundamental driving force for the quantum decoherence of $^1(T_1T_1)$ is its interaction with its dissipative environment, which is typically described by a thermalized phonon path at finite temperature (Tao, 2014). This system-environment interaction varies greatly from amorphous, or polycrystalline, to ordered crystalline structures. Singlet fission materials in the form of single crystal are anticipated to exhibit pronounced collective characteristics in molecular vibrations because of their ordered crystalline structures.

In this work, we investigated the quantum decoherence of $^1(T_1T_1)$ states in single crystalline hexacene by polarized transient absorption spectroscopy in conjunction with *ab initio* quantum mechanics simulations. Our results showed that both $^1(T_1T_1)$ and T_1+T_1 states are of anisotropic origin owing to triplet Davydov splitting in hexacene, leading to distinctive quantum decoherence rates along crystal ***a*** and ***b*** axes. This notable anisotropy can be principally ascribed to the difference on the energy gap between $^1(T_1T_1)$ and T_1+T_1 according to the Redfield quantum dissipation theory (Ishizaki and Fleming, 2009). Moreover, through our functional mode analysis, the anisotropic quantum decoherence is predominantly driven by some slow phonon modes with an effective frequency $\omega_p < 50\ cm^{-1}$.

RESULTS

Singlet Davydov Splitting in Hexacene

Hexacene single crystals used in our experiments were grown with physical vapor transport by following a recently developed method (Laudise et al., 1998; Watanabe et al., 2012). Their typical lateral size was on the order of 20 μm × 40 μm (Figure 1A), whereas their thickness was estimated to be 0.5 μm as detailed in Supplemental Information. The triclinic unit cell of hexacene shown in Figure 1B is defined by experimental in-plane crystal lattice constants (Watanabe et al., 2012) of ***a*** = 7.673 Å (long axis) and ***b*** = 6.292 Å (short axis) (Yamagata et al., 2011). A home-built microscopy was coupled with a tungsten-halogen light source for polarization-dependent optical transmission measurements of hexacene single crystal (Figure S1), and its polarization-resolved linear absorption spectra for the ***ab*** plane is presented on Figure 1C. Interestingly, the polarized measurements exhibit different absorption features along these two lattice axes. The lowest resonant peak at 835 nm was assigned to be the transition along the short ***b*** axis and is called $\boldsymbol{b_1}$. On

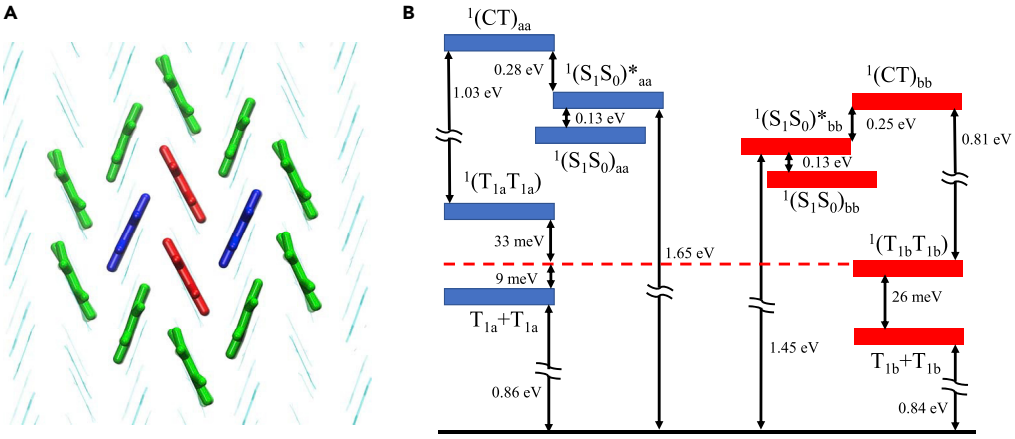

Figure 2. Supercell and Energy Diagram of all Spin States for Hexacene Single Crystal

(A) 9 × 9 × 3 supercell of a hexacene single crystal. The tetramer designated as the singlet fission reaction center is highlighted. The molecular pair along the crystal ***a*** axis is colored blue, whereas the one along the crystal ***b*** axis is colored red. Moreover, all nearest neighbors of the tetramer are colored green.

(B) Energy diagram of all spin states participating in the single-fission process. The ground state, singlet excited state, charge-transfer state, correlated triplet pair, and uncorrelated triplet dimer are denoted as S_0S_0, S_1S_0, CT, $^1(T_1T_1)$, and $T_1 + T_1$, respectively. Their subscripts of ***a*** and ***b*** refer to the corresponding crystal axes. For instance, $^1(T_{1a}T_{1a})$ represents a correlated triple pair whose constituents are along the [100] crystal axis.

the other hand, the lowest transition at 761 nm was attributed to the transition along the long ***a*** axis and is named $\boldsymbol{a}_1$. Apparently, $\boldsymbol{b}_1$ is redshifted by 144 meV (1,160 cm^{-1}) with respect to $\boldsymbol{a}_1$. This notable energy difference is due to the splitting of electronic excitations, the so-called singlet Davydov splitting (Davydov, 1948, 2013) that stems from dipole-dipole interactions of two non-equivalent molecules in a hexacene unit cell (Chernikov et al., 2014; Hestand et al., 2015).

Calculated Anisotropic Energy Levels in Hexacene Single Crystals

To explore the energy levels of all singlet-fission participating states in single crystalline hexacene, we performed computer simulations under periodic boundary conditions. Specifically, the single crystalline hexacene was modeled as a 9 × 9 × 3 supercell with a total of 20,412 atoms (Figure 2A). For a compromised balance between numerical efficiency and physical accuracy, the hybrid quantum mechanics/molecular mechanics approach (Warshel and Levitt, 1976) was adopted. A detailed description of the computational calculations can be found in Supplemental Information. As shown in Figure 2B, we denote the ground state, singlet excited state, charge-transfer state, correlated triplet pair, and decoupled triplet dimer as $^1(S_0S_0)$, $^1(S_1S_0)$, CT, $^1(T_1T_1)$, and $T_1 + T_1$, respectively, and their constituent spin configurations were illustrated in our previous studies (Elenewski et al., 2017a, 2017b). Geometry optimization was carried out on all spin states before their relative energies are determined. The only exception is $^1(S_1S_0)^*$, which assumes the same geometry as $^1(S_0S_0)$, such that $\Delta E(S_0S_0 \rightarrow S_1S_0^*)$ reflects the vertical optical gap of hexacene crystal. In particular, the linear-response time-dependent density functional theory(Casida and Huix-Rotllant, 2012) was utilized to delineate the $^1(S_1S_0)$ and $^1(S_1S_0)^*$ states, whereas the constrained density functional theory (CDFT) (Kaduk et al., 2012) was used to construct the reference orbitals needed for the multi-configurational *CT*, $^1(T_1T_1)$, and $T_1 + T_1$ states. As for the $T_1 + T_1$ dimer, a correction term of $-k_bT\ln(3 \times 3) \approx -56$ meV was added to account for the electronic spin entropy. Interestingly, we found that the $^1(T_1T_1)$ and $T_1 + T_1$ states along the short ***b*** axis are more thermodynamically stable than their counterparts along the long ***a*** axis, suggesting possible directional heterogeneity of quantum decoherence.

Spectroscopic Signatures of Triplet Davydov Splitting

Transient absorption spectroscopy is a proven tool to investigate singlet fission in solution and in thin film. We have designed and constructed a polarization-resolved transient absorption microscopy to examine anisotropic singlet fission in hexacene single crystals. A detailed description of our experimental setup is presented in Figure S1. In short, a regenerative amplifier Ti:Sapphire laser system operating at 795 nm and 1 kHz repetition rate was used for our measurements. A small portion of the laser pulse was taken as a pump light, and its fluence on samples was kept below 200 $\mu J/cm^2$ to avoid exciton-exciton

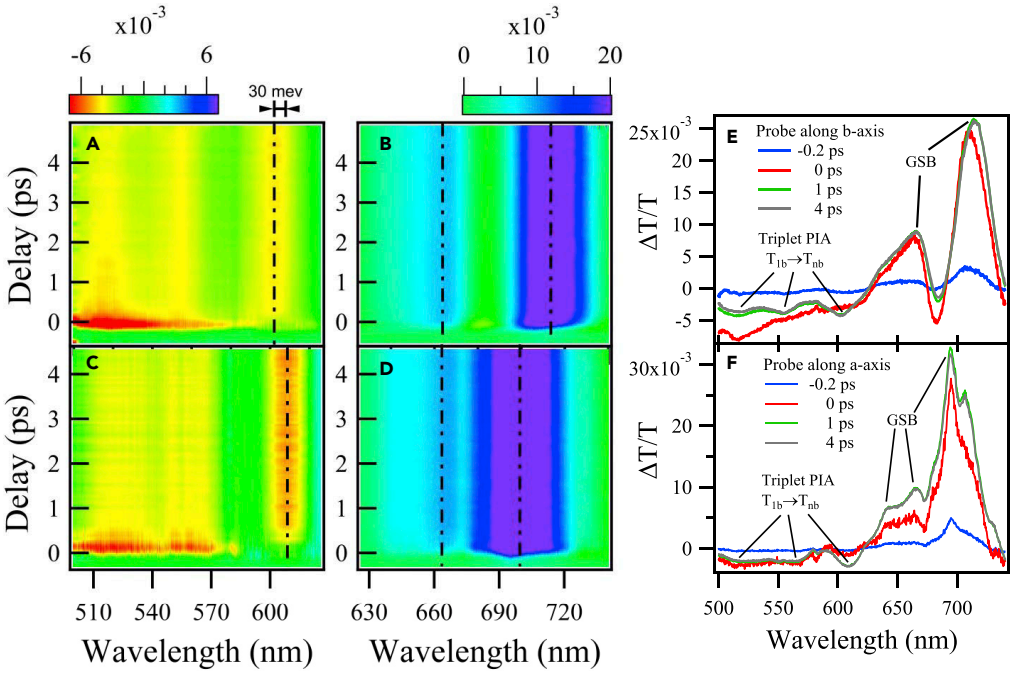

Figure 3. Polarized Transient Absorption Spectra of Hexacene Single Crystal

(Left) Pseudo-color plots of polarized transient absorption spectra from hexacene single crystal excited at 795 nm along the ***b*** crystalline axis and probing along the ***b*** axis (A and B) and along the ***a*** axis (C and D). Note that the color scales for (B) and (D) (ground state bleaching, 620 nm–738 nm) and (A) and (C) (excited state absorption, 500 nm–626 nm) are comparison sake. For a better contrast, the color scale for (D) has been multiplied by 1.75. (Right) Transient absorption spectra at several time delays probing the ***b*** axis (E) and along the ***a*** axis (F).

annihilation (Figure S3) by using a half-wave plate and a polarizer. Another small part of the laser pulse with a pulse energy of ca. 1 μJ was focused onto a sapphire crystal to generate white light supercontinuum as a probe. The pump and probe beams were combined to become collinear with a pellicle beam splitter. They were then focused onto samples through a 10× microscope objective. The polarizations of the pump and probe beams were independently adjusted with two individual half-wave plates.

To explore anisotropic spectral kinetics in hexacene single crystals, polarization-resolved transient absorption measurements were performed along both axes using a pump along ***b*** axis under the near lowest photo-excitation of 795 nm. Their results were presented as pseudo-color plots of transient absorption spectra (ΔT/T) along ***b*** axis (Figures 3A and 3B) and ***a*** axis (Figures 3C and 3D). We chose two different color scales to highlight the difference on relaxation between the perturbed ground state and the newly populated excited states. The strong positive changes in ΔT/T between 729 and 620 nm were primarily due to the ground state bleaching and recovery. As expected, these positive responses ΔT/T in spectra are similar to those of the linear absorption spectra in hexacene as shown in Figure 1C. The negative spectral changes in ΔT/T between 496 and 620 nm were attributed to the photo-induced absorption of the excited states (Figures 3E and 3F). The transient spectra along both axes have broad, featureless, and short-lived bands from 496 to 577 nm (Figures 3E and 3F). The fast process dominated in this spectral region can be ascribed to the excited state absorption S_1 to a higher singlet state S_n ($S_1 \rightarrow S_n$). By contrast, long-lived peaks appear in the range between 590 and 620 nm, as well as in the range between 508 and 544 nm. The latter even overlaps with the short-lived bands. We attributed these long-lived peaks to triplet transitions in hexacene. Again, a strong anisotropicity was observed on the triplet transitions. The peak along ***b*** axis is at 599 nm, whereas the one along ***a*** axis is redshifted by 9 nm. Since the redshift is an indicator of triplet Davydov splitting, we expect a coexistence of two kinds of triplet excitons with a splitting energy of 30 meV. Note that the correlated triplet pair, $^1(T_1T_1)$, is a dark state in our case and did not show appreciable spectral feature in the transient spectra. Therefore, the 9-nm redshift must be induced by the energy difference between the decoupled triplet dimers, i.e., $T_{1a} + T_{1a}$ and $T_{1b} + T_{1b}$. Interestingly, $T_{1b} + T_{1b}$ was found to be energetically more stable than $T_{1a} + T_{1a}$ probably due to the stronger Davydov splitting between two spatially closer

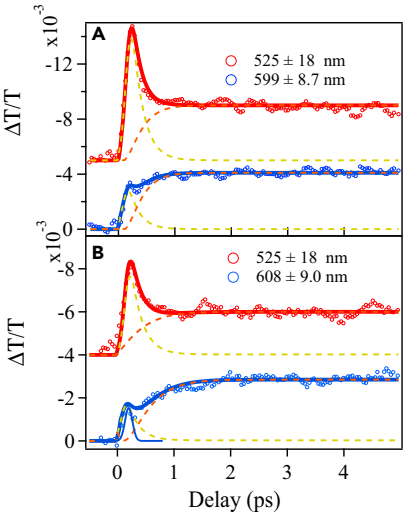

Figure 4. Kinetics Traces in the Transmission Change ΔT/T along the *a* and *b* Axes

(A and B) (A) At 525 ± 18.0 and 599 ± 8.7 nm probing along the ***b*** axis and (B) at 525 ± 18.0 and 608 ± 9.0 nm probing along the ***a*** axis, under 795 nm with a pump polarization along the ***b*** axis. Global fittings of the kinetic traces to the two-step model described in the context yield the generation and dissociation rates for the $^1(T_1T_1)$ along the ***b*** axis ($k_{F,b} = 4.5 \pm 0.2\,ps^{-1}$, $k_{Q,b} = 6.7 \pm 0.2\,ps^{-1}$) and the ***a*** axis ($k_{F,a} = 5.0 \pm 0.2\,ps^{-1}$, $k_{Q,a} = 3.3 \pm 0.2\,ps^{-1}$), respectively. The instrumental response function was 130 fs.

triplet excitons. Nevertheless, the long-lived spectral features between 500 and 620 nm were assigned to the $T_1 \rightarrow T_n$ transitions along both axes (Busby et al., 2014; Lee et al., 2013).

Moreover, we measured the anisotropic transient spectra using pumps along both axes to further verify the independence of triplet Davydov splitting on pump polarization. The independence was confirmed by Figure S4, which does not manifest appreciable change when the pump polarization is varied. Furthermore, we changed the excitation wavelengths to 400 nm and again observed distinctive triplet Davydov splitting (Figure S12). Therefore, the anisotropy of the triplet states and their derivatives is an intrinsic property of crystalline hexacene regardless of external electromagnetic perturbations.

Singlet Fission Kinetics along the Long and Short Crystal Axes

Figure 4 shows kinetic traces of hexacene in terms of ΔT/T after pumps are applied along ***b*** axis with the following wavelengths: (1) 525 ± 18.0 nm for $S_1 \rightarrow S_n$; (2) 599 ± 8.7 nm for $T_{1b} \rightarrow T_{nb}$; (3) 608 ± 9.0 nm for $T_{1a} \rightarrow T_{na}$. A kinetic model (Johnson et al., 2010; Monahan et al., 2017; Wan et al., 2018) was used to derive the generation and dissociation rates of $^1(T_1T_1)$ state from the experimental data shown in Figure 4. The detailed fitting procedure can be found in Supplemental Information. A global fitting of the kinetic traces affords the formation (k_F) and decoherence (k_Q) rates along ***b*** axis as $k_{F,\,bb} = 4.5 \pm 0.2\,ps^{-1}$ and $k_{Q,\,bb} = 6.7 \pm 0.2\,ps^{-1}$, respectively. Similarly, their counterparts along ***a*** axis are given by $k_{F,aa} = 5.0 \pm 0.2\,ps^{-1}$ and $k_{Q,\,aa} = 3.3 \pm 0.2\,ps^{-1}$. Apparently, k_F remains nearly unchanged, whereas k_Q has more than doubled after the probe polarization rotates from ***a*** axis to ***b*** axis. Once again, our experimental data suggest that the mechanism of singlet fission is of anisotropic nature in single crystalline hexacene.

DISCUSSION

Our studies of single crystalline hexacene have three main traits: (1) a large triplet Davydov splitting of 30 meV; (2) a homogeneous $^1(T_1T_1)$ formation rate regardless of molecular directionality; (3) a notable anisotropy of $^1(T_1T_1)$ quantum decoherence rate. We have also proposed a unified vibronic model for singlet fission by treating the formation of a correlated triplet pair and its quantum decoherence on the same footing using our non-adiabatic functional mode approach (Chen, 2014; Elenewski et al., 2017b). As clearly depicted in Scheme 1, the optical excitation results in anisotropic structural and dynamical properties for both the $^1(T_1T_1)$ and $T_1 + T_1$ states, allowing us to gain more insights into the intrinsic directional heterogeneity of triplet excitons in single crystalline hexacene.

Formation of $^1(T_1T_1)$ Directly from $^1(S_1S_0)^*$

The formation of $^1(T_1T_1)$ is generally considered as the rate-determining step of singlet fission under the assumption of ultrafast quantum decoherence of $^1(T_1T_1)$. Surprisingly, our results show that the formation

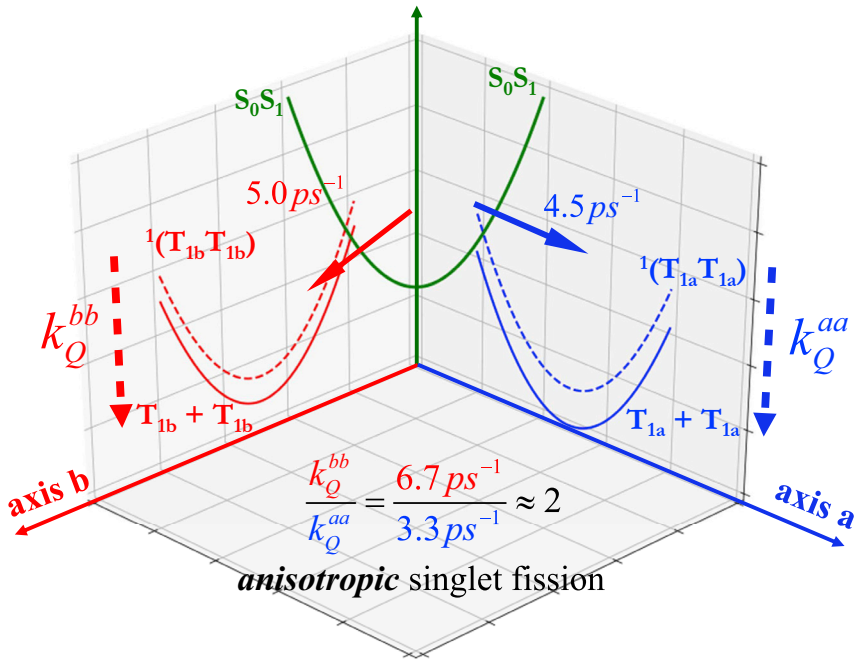

Scheme 1. Schematic for Anisotropic Singlet Fission in Hexacene Single Crystal

Anisotropic $^1(T_1T_1)$ states are formed along the short ***b*** and long ***a*** axes **directly** from the hot S_1S_0 state. The rate for quantum decoherence along the short ***b*** axis is almost twice that along the long ***a*** axis. $^1(T_{1a}T_{1a})$ and $^1(T_{1b}T_{1b})$ represent correlated triplet pair states along the ***a*** and ***b*** axes, whereas $T_{1a} + T_{1a}$ and $T_{1b} + T_{1b}$ are triplet states along the ***a*** and ***b*** axes.

of $^1(T_1T_1)$ outpaces its quantum decoherence in hexacene, making the overall singlet fission rate predominantly decided by the latter. More interestingly, the formation rates of $^1(T_1T_1)$ were found to be similar along ***b*** axis ($k_{F,\,bb} = 4.5 \pm 0.2\ ps^{-1}$) and ***a*** axis ($k_{F,aa} = 5.0 \pm 0.2\ ps^{-1}$). As previously discussed, the formation of $^1(T_1T_1)$ could proceed through the direct, the CT-mediated, and the sequential mechanisms. To reconcile which mechanism is responsible for the fast and isotropic formation of $^1(T_1T_1)$ in hexacene, we employed our functional mode vibronic theory that has been successfully applied to investigate singlet fission in tetracene and pentacene (Elenewski et al., 2017a, 2017b). If the direct mechanism is followed, $^1(T_1T_1)$ is formed without the aid of any CT intermediate. By contrast, the sequential mechanism demands a thermodynamically stable CT state with an energy lower than the hot $^1(S_1S_0)^*$. Similarly, the mediated mechanism entails a virtual CT state, whose energy should be close to $^1(S_1S_0)^*$ for an ideal vibrational wave-function mixing between them. Since our calculated energy diagram in Figure 2 manifests a relatively large energy gap of over 0.25 eV between the CT and $^1(S_1S_0)^*$ states, both the sequential and mediated mechanisms should be effectively blocked. In this regard, we assume that the $^1(T_1T_1)$ pair production in single crystalline hexacene only proceeds through the direct mechanism (Elenewski et al., 2016, 2017b):

$$k_F = \frac{J^2}{\hbar^2}\int_{-\infty}^{+\infty} e^{\frac{i\left(\Delta G_0 + \lambda - \hbar\Omega n(0)e^{-\Gamma|t|}\right)t}{\hbar}} e^{-\frac{1}{2}\Omega^2 t^2} e^{-n(0)e^{-\Gamma|t|}\Omega^2 t^2}\, dt \qquad \text{(Equation 2)}$$

where J is the electronic strength between $^1(S_1S_0)^*$ and $^1(T_1T_1)$, $\Delta G_0 = E_{S_0S_1} - E_{(TT)}$ is the driving force of singlet fission, λ is the associated reorganization energy, Ω is the angular frequency of the effective singlet-fission driving vibrational mode, Γ is its thermal relaxation rate, and $n(0) = E_{inc} - E_{S_0S_1}/\hbar\Omega$ is the optically populated initial vibrational quanta where E_{inc} is the incident light energy, which is 795 nm in the present study. We can then apply Equation 2 to calculate the $^1(T_1T_1)$ formation rate k_F under non-thermalized condition. It was found that $k_{F,aa}$ of 0.93 ps^{-1} is nearly the same as $k_{F,bb}$ of 0.83 ps^{-1}, in spite of a modest disparity in energetic parameters such as ΔG_0 and λ. The diminished difference on k_S along ***a*** and ***b*** axes primarily arises from their fast Ωs, whose zero-point energies become much more overwhelming for vibrational quantum tunneling. As suggested by Busby et al., 2014, almost all singlet excitons in hexacene crystal undergo singlet fission, resulting in a triplet quantum yield of nearly 200% that also affords a

negligible fluorescence quantum yield. If so, the overall decay rate, k_D, of $^1(S_1S_0)^*$ is simply $k_F + \Gamma$, leading to $k_{D,aa}$ of 1.86 ps^{-1} and $k_{D,bb}$ of 2.08 ps^{-1}. These computed rates are in good agreement with those obtained from our experimental measurements, indicating a direct formation of $^1(T_1T_1)$ from the vibrationally "hot" $^1(S_1S_0)^*$ in hexacene. In fact, previous studies of hexacene thin films attributed a slower singlet fission to multi-phonon relaxations, as compared with pentacene and tetracene (Busby et al., 2014). For example, ultrafast vibronic spectroscopies of pentacene and its derivatives showed that the singlet fission process is a single-molecular internal conversion via a conical intersection due to strong coupling between nuclear and electronic motions (Musser et al., 2015). As a result, the thermal relaxation of the $^1(S_1S_0)^*$ state should be taken into account when its decay rate is probed by transient spectroscopy techniques.

Anisotropic Nature of $T_1 + T_1$ and $^1(T_1T_1)$

Triplet Davydov splitting exhibits a difference in energy as high as 30 meV along the ***a*** and ***b*** axes in hexacene single crystals, indicating that the $T_1 + T_1$ states remain strong dipole-dipole interactions in the anisotropic environment. The energy level of $T_{1b} + T_{1b}$ is lower than that of $T_{1a} + T_{1a}$ in the case of hexacene. This energy alignment is opposite to that of pentacene (Figure S5) and tetracene (Schwoerer and Birech, 2014), both of which have $T_{1b} + T_{1b}$ higher than $T_{1a} + T_{1a}$ as reported. Since the anisotropic lowest spin-correlated triplet $T_1 + T_1$ states arises from the decoherence of $^1(T_1T_1)$, it is legitimate to surmise that the $^1(T_1T_1)$ states should be anisotropic in hexacene single crystals. We further hypothesized that the energy level for $^1(T_{1b}T_{1b})$ is lower than that for $^1(T_{1a}T_{1a})$ in hexacene single crystals from the measured triplet Davydov splitting.

To reveal the nature of the anisotropic $^1(T_1T_1)$ and $T_1 + T_1$ states, we need to address the anti-ferromagnetic electron correlation in acenes as revealed by a complete active space simulation using the density matrix renormalization group algorithm (Hachmann et al., 2007). This anti-ferromagnetism was later corroborated by a spin-polarized density functional theory study (Jiang and Dai, 2008), which discovered spatially separated magnetizations in acenes. Similarly, electron spins in hexacene favor anti-ferromagnetic correlation, resulting in the notable presence of diradical covalence resonance structures. For example, a pair of adjacent hexacene molecules along ***a*** axis had been extracted from the crystal structure before a complete active space self-consistent field calculation (Aquilante et al., 2016) with an active space of CAS(6,6) was conducted to reveal an enthalpy difference, $E_{(T_1+T_1)_{aa}} - E_{(T_1T_1)_{aa}}$, of 16.7 meV. In fact, a similar value of 13.5 meV was also achieved by our employed CDFT method that had been demonstrated to achieve a comparable accuracy against the multireference configuration interaction MRCI + Q level of theory on polyacenes (Kubas et al., 2014). Since a $T_1 + T_1$ dimer has less anti-ferromagnetic characteristics than its parental $^1(T_1T_1)$ pair in spite of more available spin microstates, its relative energetic stability is determined by a direct competition between enthalpy and entropy, i.e., $E_{HS\rightarrow LS}$ *versus* $k_BT\ln 9$. It turns out that entropy is a more dominant factor than enthalpy for crystalline hexacene at room temperature, making $T_1 + T_1$ thermodynamically more stable than $^1(T_1T_1)$ as shown in Figure 2. By the same token, the $^1(T_{1a}T_{1a})$ pair is expected to have a higher energy than its counterpart along axis *b* owing to diminished anti-ferromagnetic coupling strength over distance. Nevertheless, the difference on the spin-flip energy between the two axes is not strong enough to override their gap on the $^1(T_1T_1)$ pair, thus sustaining the relative stability of $T_{1b} + T_{1b}$ over $T_{1a} + T_{1a}$.

In polycrystalline singlet fission materials, the anisotropy of the $^1(T_1T_1)$ states may preserve within individual crystalline grains. The random orientation of those grain boundaries, however, is bound to suppress the global expression of the anisotropy. Very uniquely, our studies in the form of single crystals allow us to unravel the anisotropic nature of the $^1(T_1T_1)$ state without ambiguity. Previous studies of polycrystalline acenes and other singlet fission materials showed that the energy level of a triplet pair $^1(T_1T_1)$ is higher than that of a decoupled triplet dimer(Basel et al., 2019; Yong et al., 2017). Recently, a triplet pair $^1(T_1T_1)$ was reported to be bound relative to free triplets with an energy of ca. 30 meV, which is largely material independent (Yong et al., 2017). Our results not only demonstrated a higher energy of $^1(T_1T_1)$ than $T_1 + T_1$, but also exhibit their anisotropic features in hexacene.

Anisotropic Quantum Decoherence of $^1(T_1T_1)$

The transition dipole strength for the triplet pair $^1(T_1T_1)$ state is generally too weak to be detected so that its quantum decoherence is usually assumed to be much faster than its formation (Berkelbach et al., 2014; Chan et al., 2013; Coto et al., 2015; Mirjani et al., 2014; Tamura et al., 2015; Yost et al., 2014). Nevertheless, some studies implied that the quantum decoherence rate of the $^1(T_1T_1)$ state could be as slow as its formation rate (Feng and Krylov, 2016; Kolomeisky et al., 2014; Monahan et al., 2017; Pensack et al., 2016). In the

present study, we found that k_Q is even slower than k_F along the long ***a*** axis, whereas k_Q along the short ***b*** axis is comparable with k_F. Our results indicate that the relatively slow quantum decoherence is as important as triplet pair formation for the overall singlet fission rate in hexacene. According to the Redfield quantum dissipation theory (Ishizaki and Fleming, 2009), the quantum decoherence rate, k_Q, due to system-bath coupling is given by:

$$k_Q \approx \frac{2\lambda\omega_p \Delta E}{\Delta E^2 + \hbar^2\omega_p^2}\left(\frac{e^{\frac{\Delta E}{k_b T}}}{e^{\frac{\Delta E}{k_b T}} - 1}\right) \qquad \text{(Equation 3)}$$

where ΔE is the energy gap between the initial and final states of quantum decoherence, λ is the corresponding reorganization energy, and ω_p is the system-bath coupling frequency. If the quantum decoherence of $^1(T_1T_1)$ pair in hexacene crystal is assumed to be driven by vibronic coupling only, ω_p can be ascertained by the functional mode analysis (Hub and de Groot, 2009), which projects the diabatic energy gaps between $^1(T_1T_1)$ and $T_1 + T_1$ onto the dimer's vibrational normal modes for 5,000 snapshots extracted from our MD trajectory. It was found that the quantum decoherence is predominantly driven by a few slow vibrational modes with $\omega_p < 50\ cm^{-1}$ (Figure S11). Thus, the quantum decoherence is mediated by the electron-phonon interaction in crystalline hexacene. Even if we account for the small contributions from other vibrational modes that are usually much faster, the calculated effective driving mode, $\omega_p = (\sum_{i=1}^{N_{vib}} c_i^2 \omega_i^{-1})$, is still as slow as $\sim 40\ cm^{-1}$ (Table S3). Therefore, ω_p is an important factor for the quantum decoherence of $^1(T_1T_1)$ pair in hexacene because of its notable mismatch with ΔE, i.e., $\hbar\omega_p \ll \Delta E \rightarrow k_Q \propto \omega_p \lambda \Delta E^{-1}$. Interestingly, the ΔE along ***a*** axis is nearly two times as large as its counterpart along ***b*** axis, resulting in a remarkable directional heterogeneity of k_D, i.e., $\frac{k_{Q,bb}}{k_{Q,aa}} \approx 1.7$. Besides the experimentally consistent heterogeneity factor, our calculated values of k_Q along the two crystal axes are also well in line with the results from our ultrafast spectroscopy studies (Table S2).

Previous studies of singlet fission in pentacene and hexacene were performed on their polycrystalline films (Bakulin et al., 2016; Busby et al., 2014; Chan et al., 2011; Kandada et al., 2014; Rao et al., 2011; Wilson et al., 2011, 2013). Fission rates of the films are, in general, the averaged result over different orientations of the polycrystalline structures, leading to a loss of intrinsically anisotropic features in these materials. Transient absorption microscopy experiments found that long-lived correlated triplet pairs exist and triplet interaction and binding could be induced by a π-staked geometry in crystalline pentacene derivative (Folie et al., 2018). Polarization measurements of tetracene demonstrated that there was no difference in kinetics along the long and short axes (Schwoerer and Birech, 2014; Wan et al., 2015; Zhang et al., 2014). By contrast, our results showed that the anisotropic quantum decoherence of $^1(T_1T_1)$ occurs in single crystalline hexacene. This decoherence process is driven by the vibronic coupling between the $^1(T_1T_1)$ state and some low-frequency phonon modes of hexacene crystal. Owing to the directional asymmetry of the crystal, this quantum decoherence process might be intrinsically anisotropic as governed by the energy gap between $^1(T_1T_1)$ and $T_1 + T_1$.

In summary, we discovered anisotropic singlet fission in single crystalline hexacene and have revealed its mechanism by deciphering its two constituent steps. For the first step that gives rise to correlated triplet pairs through the so-called direct mechanism, no anisotropy was found as they were formed on the same timescale of ~200 fs along the two crystal axes. In the second step that involves quantum decoherence of the correlated triplet pairs, the rate along the short ***b*** axis is nearly two times as fast as that along the long ***a*** axis. The difference on the rate might be ascribed to the directional heterogeneity of the hexacene crystal that results in distinct thermodynamic stabilities between the initial and final states of the quantum decoherence, which is driven by system-bath coupling with a slow effective frequency of $\omega_p < 50\ cm^{-1}$. Our findings not only corroborated the importance of quantum decoherence in fission process, but will also guide future experimental and theoretical endeavors of exploring anisotropic photophysical properties in novel materials for multiple exciton generation.

Limitations of the Study

From a fundamental point of view, one of the most challenging tasks for the singlet fission community is the characterization and monitoring of the optically dark $^1(T_1T_1)$ state due to its small absorption cross section and short lifetime upon photo-excitation. Although the transient absorption spectra of the $^1(T_1T_1)$ state were presented in recent experiments (Burdett and Bardeen, 2012; Korovina et al., 2016; Lukman et al.,

2015, 2016, Stern et al., 2015, 2017), those results are limited to intramolecular singlet fission or intermolecular one for dimers in solution (Rao and Friend, 2017) with unusually long $^1(T_1T_1)$ lifetime. Therefore, it is not surprising that the optical identification of the short-lived $^1(T_1T_1)$ state in hexacene has not been reported yet with the transient absorption spectroscopy method. More recently, the two-dimensional optical spectroscopy was employed to demonstrate the existence of $^1(T_1T_1)$ state in thin film pentacene and its derivatives (Bakulin et al., 2016). Nevertheless, this technique has to be coupled with a microscopy approach for small-size samples such as single crystalline hexacene, our system of interest.

METHODS

All methods can be found in the accompanying Transparent Methods supplemental file.

SUPPLEMENTAL INFORMATION

Supplemental Information can be found online at https://doi.org/10.1016/j.isci.2019.08.053.

ACKNOWLEDGMENTS

This work was supported by the Honda Research Institute (Ohio) before June 1, 2015, by Air Force Office of Scientific Research (AFOSR) (FA9550-15-1-0213) between June 1, 2015, and July 31, 2017, and by Utah State University after August 1, 2017. D.S. was supported by the W. M. Keck Foundation. Computational resources were provided by the Argonne Leadership Computing Facilities at Argonne National Laboratory under Department of Energy contract DE-AC-06CH11357 and by the Extreme Science and Engineering Discovery Environment at Texas Advanced Computing Center under National Science Foundation contract TG-CHE130008. Y.R. thank Drs. Tony F. Heinz, Omer Yaffe, Xiaoyang Zhu, and Francis Spano for their beneficial discussion.

AUTHOR CONTRIBUTIONS

D.S., G.-H.D., B.X., Y.W., and Y.Q. performed the transient absorption measurements and characterizations. E.X. performed the theoretical calculation. X.L. and Y.Z. prepared the samples. D.S., G.-H.D., B.X., C.N., A.R.H., H.-L.D., G.C., H.C., and Y.R. analyzed the data. Y.R., G.C., A.R.H., H.C., C.N., and H.-L.D. designed the project. Y.R., G.C., C.N., A.R.H., and H.-L.D. supervised the experiments. H.C. supervised the theoretical calculation. D.S, G.-H.D, B.X., and E.X. wrote the original draft. Y.R., H.C., and G.C. revised the manuscript.

DECLARATION OF INTERESTS

The authors declare no competing interests.

Received: April 24, 2019
Revised: July 1, 2019
Accepted: August 26, 2019
Published: September 27, 2019

REFERENCES

Aquilante, F., Autschbach, J., Carlson, R.K., Chibotaru, L.F., Delcey, M.G., De Vico, L., Fdez Galván, I., Ferré, N., Frutos, L.M., Gagliardi, L., et al. (2016). Molcas 8: new capabilities for multiconfigurational quantum chemical calculations across the periodic table. J. Comput. Chem. *37*, 506–541.

Bakulin, A.A., Morgan, S.E., Kehoe, T.B., Wilson, M.W.B., Chin, A.W., Zigmantas, D., Egorova, D., and Rao, A. (2016). Real-time observation of multiexcitonic states in ultrafast singlet fission using coherent 2D electronic spectroscopy. Nat. Chem. *8*, 16–23.

Basel, B.S., Papadopoulos, I., Thiel, D., Casillas, R., Zirzlmeier, J., Clark, T., Guldi, D.M., and Tykwinski, R.R. (2019). Pentacenes: a molecular Ruler for singlet fission. Trends Chem. *1*, 11–21.

Beljonne, D., Yamagata, H., Bredas, J.L., Spano, F.C., and Olivier, Y. (2013). Charge-transfer excitations steer the Davydov splitting and mediate singlet exciton fission in pentacene. Phys. Rev. Lett. *110*, 226402.

Berkelbach, T.C., Hybertsen, M.S., and Reichman, D.R. (2013a). Microscopic theory of singlet exciton fission. I. General formulation. J. Chem. Phys. *138*, 114102.

Berkelbach, T.C., Hybertsen, M.S., and Reichman, D.R. (2013b). Microscopic theory of singlet exciton fission. II. Application to pentacene dimers and the role of superexchange. J. Chem. Phys. *138*, 114103.

Berkelbach, T.C., Hybertsen, M.S., and Reichman, D.R. (2014). Microscopic theory of singlet exciton fission. III. Crystalline pentacene. J. Chem. Phys. *141*, 074705.

Burdett, J.J., and Bardeen, C.J. (2012). Quantum beats in crystalline tetracene delayed fluorescence due to triplet pair coherences produced by direct singlet fission. J. Am. Chem. Soc. *134*, 8597–8607.

Burdett, J.J., Muller, A.M., Gosztola, D., and Bardeen, C.J. (2010). Excited state dynamics in solid and monomeric tetracene: the roles of

superradiance and exciton fission. J. Chem. Phys. *133*, 144506.

Busby, E., Berkelbach, T.C., Kumar, B., Chernikov, A., Zhong, Y., Hlaing, H., Zhu, X.Y., Heinz, T.F., Hybertsen, M.S., Sfeir, M.Y., et al. (2014). Multiphonon relaxation slows singlet fission in crystalline hexacene. J. Am. Chem. Soc. *136*, 10654–10660.

Busby, E., Xia, J., Wu, Q., Low, J.Z., Song, R., Miller, J.R., Zhu, X.Y., Campos, L.M., and Sfeir, M.Y. (2015). A design strategy for intramolecular singlet fission mediated by charge-transfer states in donor-acceptor organic materials. Nat. Mater. *14*, 426–433.

Casanova, D. (2018). Theoretical modeling of singlet fission. Chem. Rev. *118*, 7164–7207.

Casida, M.E., and Huix-Rotllant, M. (2012). Progress in time-dependent density-functional theory. Annu. Rev. Phys. Chem. *63*, 287–323.

Chan, W.L., Berkelbach, T.C., Provorse, M.R., Monahan, N.R., Tritsch, J.R., Hybertsen, M.S., Reichman, D.R., Gao, J.L., and Zhu, X.Y. (2013). The quantum coherent mechanism for singlet fission: experiment and theory. Acc. Chem. Res. *46*, 1321–1329.

Chan, W.L., Ligges, M., Jailaubekov, A., Kaake, L., Miaja-Avila, L., and Zhu, X.Y. (2011). Observing the multiexciton state in singlet fission and ensuing ultrafast multielectron transfer. Science *334*, 1541–1545.

Chan, W.L., Ligges, M., and Zhu, X.Y. (2012). The energy barrier in singlet fission can be overcome through coherent coupling and entropic gain. Nat. Chem. *4*, 840–845.

Chen, H. (2014). Functional mode electron-transfer theory. J. Phys. Chem. C *118*, 7586–7593.

Chernikov, A., Yaffe, O., Kumar, B., Zhong, Y., Nuckolls, C., and Heinz, T.F. (2014). Spectroscopic study of anisotropic excitons in single crystal hexacene. J. Phys. Chem. Lett. *5*, 3632–3635.

Congreve, D.N., Lee, J., Thompson, N.J., Hontz, E., Yost, S.R., Reusswig, P.D., Bahlke, M.E., Reineke, S., Van Voorhis, T., and Baldo, M.A. (2013). External quantum efficiency above 100% in a singlet-exciton-fission–based organic photovoltaic cell. Science *340*, 334–337.

Cook, J.D., Carey, T.J., and Damrauer, N.H. (2016). Solution-phase singlet fission in a structurally well-defined norbornyl-bridged tetracene dimer. J. Phys. Chem. C *120*, 4473–4481.

Coto, P.B., Sharifzadeh, S., Neaton, J.B., and Thoss, M. (2015). Low-lying electronic excited states of pentacene oligomers: a comparative electronic structure study in the context of singlet fission. J. Chem. Theory Comput. *11*, 147–156.

Davydov, A. (1948). Theory of absorption spectra of molecular crystals. Zh. Eksp. Teor. Fiz. *18*, 210–218.

Davydov, A. (2013). Theory of Molecular Excitons (Springer).

Elenewski, J.E., Cai, J.Y., Jiang, W., and Chen, H. (2016). Functional mode hot electron transfer theory. J. Phys. Chem. C *120*, 20579–20587.

Elenewski, J.E., Cubeta, U.S., Ko, E., and Chen, H. (2017a). Computer simulation of singlet fission in single crystalline pentacene by functional mode vibronic theory. J. Phys. Chem. C *121*, 11159–11165.

Elenewski, J.E., Cubeta, U.S., Ko, E., and Chen, H. (2017b). Functional mode singlet fission theory. J. Phys. Chem. C *121*, 4130–4138.

Feng, X.T., and Krylov, A.I. (2016). On couplings and excimers: lessons from studies of singlet fission in covalently linked tetracene dimers. Phys. Chem. Chem. Phys. *18*, 7751–7761.

Folie, B.D., Haber, J.B., Refaely-Abramson, S., Neaton, J.B., and Ginsberg, N.S. (2018). Long-lived correlated triplet pairs in a π-stacked crystalline pentacene derivative. J. Am. Chem. Soc. *140*, 2326–2335.

Hachmann, J., Dorando, J.J., Avilés, M., and Chan, G.K.-L. (2007). The radical character of the acenes: a density matrix renormalization group study. J. Chem. Phys. *127*, 134309.

Hestand, N.J., Yamagata, H., Xu, B., Sun, D., Zhong, Y., Harutyunyan, A.R., Chen, G., Dai, H.-L., Rao, Y., and Spano, F.C. (2015). Polarized absorption in crystalline pentacene: theory vs experiment. J. Phys. Chem. C *119*, 22137–22147.

Hub, J.S., and de Groot, B.L. (2009). Detection of functional modes in protein dynamics. PLoS Comput. Biol. *5*, e1000480.

Ishizaki, A., and Fleming, G.R. (2009). On the adequacy of the Redfield equation and related approaches to the study of quantum dynamics in electronic energy transfer. J. Chem. Phys. *130*, 234110.

Jiang, D.-E., and Dai, S. (2008). Electronic ground state of higher acenes. J. Phys. Chem. C *112*, 332–335.

Johnson, J.C., Nozik, A.J., and Michl, J. (2010). High triplet yield from singlet fission in a thin film of 1,3-diphenylisobenzofuran. J. Am. Chem. Soc. *132*, 16302–16303.

Jundt, C., Klein, G., Sipp, B., Lemoigne, J., Joucla, M., and Villaeys, A.A. (1995). Exciton dynamics in pentacene thin films studied by pump-probe spectroscopy. Chem. Phys. Lett. *241*, 84–88.

Kaduk, B., Kowalczyk, T., and Van Voorhis, T. (2012). Constrained density functional theory. Chem. Rev. *112*, 321–370.

Kandada, A.R.S., Petrozza, A., and Lanzani, G. (2014). Ultrafast dissociation of triplets in pentacene induced by an electric field. Phys. Rev. B *90*, 075310.

Katoh, R., Kotani, M., Hirata, Y., and Okada, T. (1997). Triplet exciton formation in a benzophenone single crystal studied by picosecond time-resolved absorption spectroscopy. Chem. Phys. Lett. *264*, 631–635.

Kolomeisky, A.B., Feng, X., and Krylov, A.I. (2014). A simple kinetic model for singlet fission: a role of electronic and entropic contributions to macroscopic rates. J. Phys. Chem. C *118*, 5188–5195.

Korovina, N.V., Das, S., Nett, Z., Feng, X., Joy, J., Haiges, R., Krylov, A.I., Bradforth, S.E., and Thompson, M.E. (2016). Singlet fission in a covalently linked cofacial alkynyltetracene dimer. J. Am. Chem. Soc. *138*, 617–627.

Kubas, A., Hoffmann, F., Heck, A., Oberhofer, H., Elstner, M., and Blumberger, J. (2014). Electronic couplings for molecular charge transfer: benchmarking CDFT, FODFT, and FODFTB against high-level ab initio calculations. J. Chem. Phys. *140*, 104105.

Laudise, R.A., Kloc, C., Simpkins, P.G., and Siegrist, T. (1998). Physical vapor growth of organic semiconductors. J. Cryst. Growth *187*, 449–454.

Lee, J., Bruzek, M.J., Thompson, N.J., Sfeir, M.Y., Anthony, J.E., and Baldo, M.A. (2013). Singlet exciton fission in a hexacene derivative. Adv. Mater. *25*, 1445–1448.

Lukman, S., Chen, K., Hodgkiss, J.M., Turban, D.H.P., Hine, N.D.M., Dong, S., Wu, J., Greenham, N.C., and Musser, A.J. (2016). Tuning the role of charge-transfer states in intramolecular singlet exciton fission through side-group engineering. Nat. Commun. *7*, 13622.

Lukman, S., Musser, A.J., Chen, K., Athanasopoulos, S., Yong, C.K., Zeng, Z., Ye, Q., Chi, C., Hodgkiss, J.M., Wu, J., et al. (2015). Tuneable singlet exciton fission and triplet–triplet annihilation in an orthogonal pentacene dimer. Adv. Funct. Mater. *25*, 5452–5461.

Marciniak, H., Pugliesi, I., Nickel, B., and Lochbrunner, S. (2009). Ultrafast singlet and triplet dynamics in microcrystalline pentacene films. Phys. Rev. B *79*, 235318.

Merrifield, R.E., Avakian, P., and Groff, R.P. (1969). Fission of singlet excitons into pairs of triplet excitons in tetracene crystals. Chem. Phys. Lett. *3*, 155–157.

Michl, J., Nozik, A.J., Chen, X., Johnson, J.C., Rana, G., Akdag, A., and Schwerin, A.F. (2007). Toward Singlet Fission for Excitonic Solar Cells. In Organic Photovoltaics VIII, Proc. SPIE, *6656* (International Society for Optics and Photonics), p. 66560E.

Mirjani, F., Renaud, N., Gorczak, N., and Grozema, F.C. (2014). Theoretical investigation of singlet fission in molecular dimers: the role of charge transfer states and quantum interference. J. Phys. Chem. C *118*, 14192–14199.

Miyata, K., Kurashige, Y., Watanabe, K., Sugimoto, T., Takahashi, S., Tanaka, S., Takeya, J., Yanai, T., and Matsumoto, Y. (2017). Coherent singlet fission activated by symmetry breaking. Nat. Chem. *9*, 983–989.

Monahan, N., and Zhu, X.-Y. (2015). Charge transfer–mediated singlet fission. Annu. Rev. Phys. Chem. *66*, 601–618.

Monahan, N.R., Sun, D., Tamura, H., Williams, K.W., Xu, B., Zhong, Y., Kumar, B., Nuckolls, C., Harutyunyan, A.R., Chen, G., et al. (2017). Dynamics of the triplet-pair state reveals the likely coexistence of coherent and incoherent singlet

fission in crystalline hexacene. Nat. Chem. *9*, 341–346.

Musser, A.J., Liebel, M., Schnedermann, C., Wende, T., Kehoe, T.B., Rao, A., and Kukura, P. (2015). Evidence for conical intersection dynamics mediating ultrafast singlet exciton fission. Nat. Phys. *11*, 352–357.

Najafov, H., Lee, B., Zhou, Q., Feldman, L.C., and Podzorov, V. (2010). Observation of long-range exciton diffusion in highly ordered organic semiconductors. Nat. Mater. *9*, 938–943.

Nakano, M., Ito, S., Nagami, T., Kitagawa, Y., and Kubo, T. (2016). Quantum master equation approach to singlet fission dynamics of realistic/artificial pentacene dimer models: relative relaxation factor analysis. J. Phys. Chem. C *120*, 22803–22815.

Pensack, R.D., Ostroumov, E.E., Tilley, A.J., Mazza, S., Grieco, C., Thorley, K.J., Asbury, J.B., Seferos, D.S., Anthony, J.E., and Scholes, G.D. (2016). Observation of two triplet-pair intermediates in singlet exciton fission. J. Phys. Chem. Lett. *7*, 2370–2375.

Rao, A., and Friend, R.H. (2017). Harnessing singlet exciton fission to break the Shockley–Queisser limit. Nat. Rev. Mater. *2*, 17063.

Rao, A., Wilson, M.W.B., Albert-Seifried, S., Di Pietro, R., and Friend, R.H. (2011). Photophysics of pentacene thin films: the role of exciton fission and heating effects. Phys. Rev. B *84*, 195411.

Schwerin, A.F., Johnson, J.C., Smith, M.B., Sreearunothai, P., Popović, D., Černý, J., Havlas, Z., Paci, I., Akdag, A., MacLeod, M.K., et al. (2010). Toward designed singlet fission: electronic states and photophysics of 1,3-diphenylisobenzofuran. J. Phys. Chem. C *114*, 1457–1473.

Schwob, H.P., and Williams, D.F. (1972). Charge transfer exciton fission in anthracene crystals. Chem. Phys. Lett. *13*, 581–584.

Schwoerer, H., and Birech, Z. (2014). Davydov splitting in triplet excitons of tetracene single crystals. In Frontiers in Optics 2014 (Optical Society of America), p. FTu1G.8.

Smith, M.B., and Michl, J. (2010). Singlet fission. Chem. Rev. *110*, 6891–6936.

Stern, H.L., Cheminal, A., Yost, S.R., Broch, K., Bayliss, S.L., Chen, K., Tabachnyk, M., Thorley, K., Greenham, N., Hodgkiss, J.M., et al. (2017). Vibronically coherent ultrafast triplet-pair formation and subsequent thermally activated dissociation control efficient endothermic singlet fission. Nat. Chem. *9*, 1205–1212.

Stern, H.L., Musser, A.J., Gelinas, S., Parkinson, P., Herz, L.M., Bruzek, M.J., Anthony, J., Friend, R.H., and Walker, B.J. (2015). Identification of a triplet pair intermediate in singlet exciton fission in solution. Proc. Natl. Acad. Sci. U S A *112*, 7656–7661.

Takeda, Y., Katoh, R., Kobayashi, H., and Kotani, M. (1996). Fission and fusion of excitons in perylene crystal studied with VUV and x-ray excitation. J. Electron. Spectrosc. Relat. Phenom. *78*, 423–425.

Tamura, H., Huix-Rotllant, M., Burghardt, I., Olivier, Y., and Beljonne, D. (2015). First-principles quantum dynamics of singlet fission: coherent versus thermally activated mechanisms governed by molecular π stacking. Phys. Rev. Lett. *115*, 107401.

Tao, G. (2014). Bath effect in singlet fission dynamics. J. Phys. Chem. C *118*, 27258–27264.

Tayebjee, M.J.Y., Clady, R., and Schmidt, T.W. (2013). The exciton dynamics in tetracene thin films. Phys. Chem. Chem. Phys. *15*, 14797–14805.

Tiago, M.L., Northrup, J.E., and Louie, S.G. (2003). Ab initio calculation of the electronic and optical properties of solid pentacene. Phys. Rev. B *67*, 115212.

Walker, B.J., Musser, A.J., Beljonne, D., and Friend, R.H. (2013). Singlet exciton fission in solution. Nat. Chem. *5*, 1019–1024.

Wan, Y., Guo, Z., Zhu, T., Yan, S., Johnson, J., and Huang, L. (2015). Cooperative singlet and triplet exciton transport in tetracene crystals visualized by ultrafast microscopy. Nat. Chem. *7*, 785–792.

Wan, Y., Wiederrecht, G.P., Schaller, R.D., Johnson, J.C., and Huang, L. (2018). Transport of spin-entangled triplet excitons generated by singlet fission. J. Phys. Chem. Lett. *9*, 6731–6738.

Warshel, A., and Levitt, M. (1976). Theoretical studies of enzymic reactions: dielectric, electrostatic and steric stabilization of the carbonium ion in the reaction of lysozyme. J. Mol. Biol. *103*, 227–249.

Watanabe, M., Chang, Y.J., Liu, S.-W., Chao, T.-H., Goto, K., Islam, M.M., Yuan, C.-H., Tao, Y.-T., Shinmyozu, T., and Chow, T.J. (2012). The synthesis, crystal structure and charge-transport properties of hexacene. Nat. Chem. *4*, 574–578.

Watanabe, S., Furube, A., and Katoh, R. (2006). Generation and decay dynamics of triplet excitons in Alq3 thin films under high-density excitation conditions. J. Phys. Chem. C *110*, 10173–10178.

Wen, X.M., Yu, P., Yuan, C.T., Ma, X.Q., and Tang, J. (2013). Singlet and triplet carrier dynamics in rubrene single crystal. J. Phys. Chem. C *117*, 17741–17747.

Wilson, M.W.B., Rao, A., Clark, J., Kumar, R.S.S., Brida, D., Cerullo, G., and Friend, R.H. (2011). Ultrafast dynamics of exciton fission in polycrystalline pentacene. J. Am. Chem. Soc. *133*, 11830–11833.

Wilson, M.W.B., Rao, A., Ehrler, B., and Friends, R.H. (2013). Singlet exciton fission in polycrystalline pentacene: from photophysics toward devices. Acc. Chem. Res. *46*, 1330–1338.

Yamagata, H., Norton, J., Hontz, E., Olivier, Y., Beljonne, D., Bredas, J.L., Silbey, R.J., and Spano, F.C. (2011). The nature of singlet excitons in oligoacene molecular crystals. J. Chem. Phys. *134*, 204703.

Yong, C.K., Musser, A.J., Bayliss, S.L., Lukman, S., Tamura, H., Bubnova, O., Hallani, R.K., Meneau, A., Resel, R., Maruyama, M., et al. (2017). The entangled triplet pair state in acene and heteroacene materials. Nat. Commun. *8*, 15953.

Yost, S.R., Lee, J., Wilson, M.W.B., Wu, T., McMahon, D.P., Parkhurst, R.R., Thompson, N.J., Congreve, D.N., Rao, A., Johnson, K., et al. (2014). A transferable model for singlet-fission kinetics. Nat. Chem. *6*, 492–497.

Zenz, C., Cerullo, G., Lanzani, G., Graupner, W., Meghdadi, F., Leising, G., and De Silvestri, S. (1999). Ultrafast photogeneration mechanisms of triplet states in para-hexaphenyl. Phys. Rev. B *59*, 14336–14341.

Zhang, B., Zhang, C., Xu, Y., Wang, R., He, B., Liu, Y., Zhang, S., Wang, X., and Xiao, M. (2014). Polarization-dependent exciton dynamics in tetracene single crystals. J. Chem. Phys. *141*, 244303.

Zimmerman, P.M., Bell, F., Casanova, D., and Head-Gordon, M. (2011). Mechanism for singlet fission in pentacene and tetracene: from single exciton to two triplets. J. Am. Chem. Soc. *133*, 19944–19952.

Zimmerman, P.M., Musgrave, C.B., and Head-Gordon, M. (2013). A correlated electron view of singlet fission. Acc. Chem. Res. *46*, 1339–1347.

Zimmerman, P.M., Zhang, Z.Y., and Musgrave, C.B. (2010). Singlet fission in pentacene through multi-exciton quantum states. Nat. Chem. *2*, 648–652.

Zirzlmeier, J., Lehnherr, D., Coto, P.B., Chernick, E.T., Casillas, R., Basel, B.S., Thoss, M., Tykwinski, R.R., and Guldi, D.M. (2015). Singlet fission in pentacene dimers. Proc. Nat. Acad. Sci. U S A *112*, 5325–5330.

ISCI, Volume *19*

Supplemental Information

Anisotropic Singlet Fission in Single Crystalline Hexacene

Dezheng Sun, Gang-Hua Deng, Bolei Xu, Enshi Xu, Xia Li, Yajing Wu, Yuqin Qian, Yu Zhong, Colin Nuckolls, Avetik R. Harutyunyan, Hai-Lung Dai, Gugang Chen, Hanning Chen, and Yi Rao

Supplemental Information

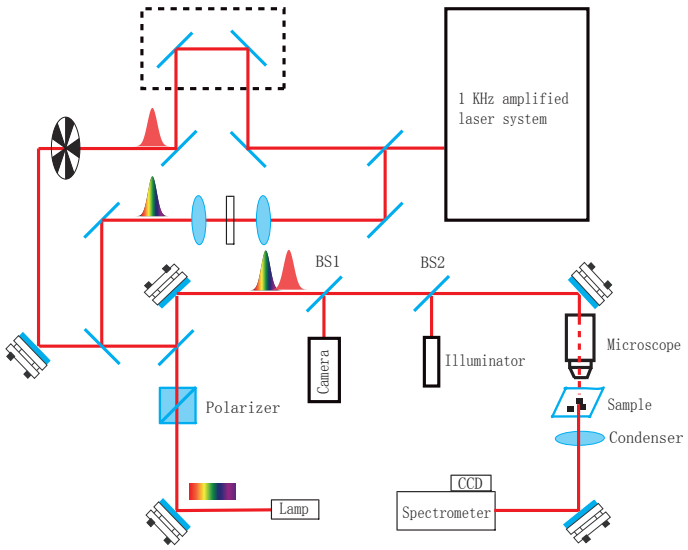

Figure S1. Schematic diagram of transient absorption setup coupled with home-built microscope. Related to Figure 1.

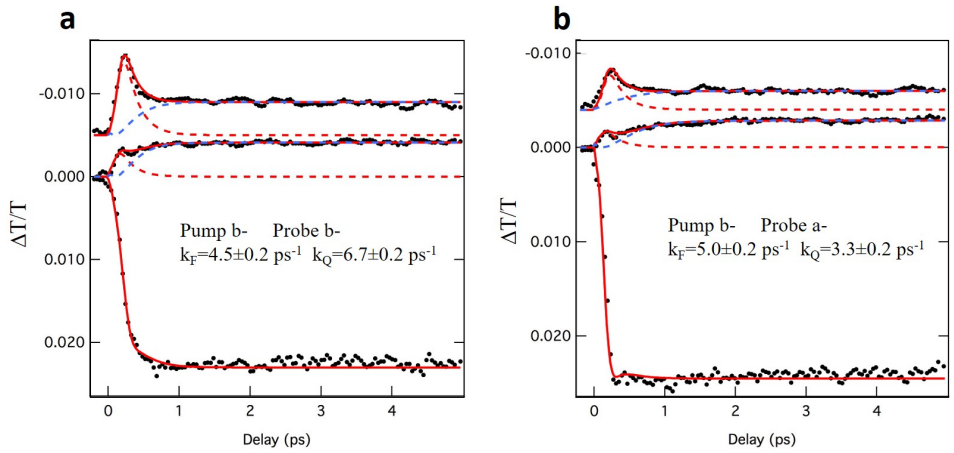

Figure S2. Global Fittings of kinetics traces with probes along ***b*** (left) and ***a*** (right) axes when the photoexcitation is applied along ***b*** axis. The dynamics has been shift vertically for clearance. The solid red line and blue line are fitted curve while the black dots are the raw data. The colored dashed lines correspond to singlet component (red) and triplet component (blue) based on the fitting results. Related to Figure 4.

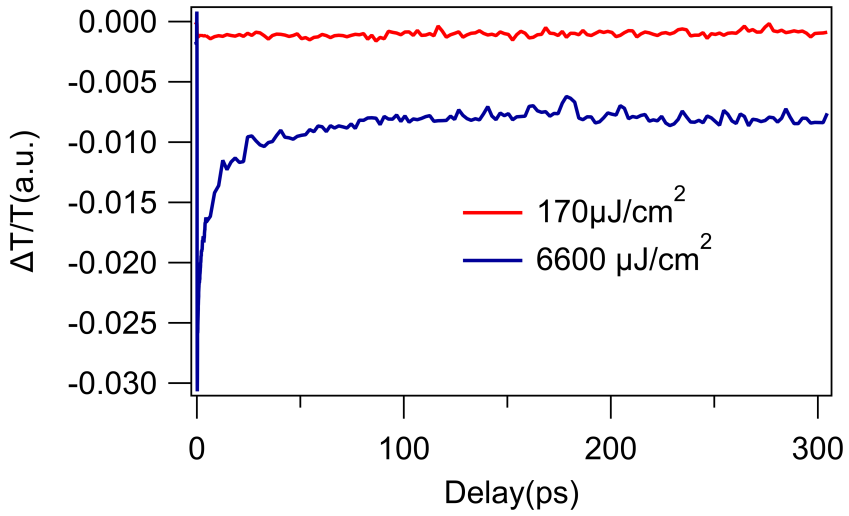

Figure S3 Triplet Exciton-Exciton Annihilation. Measured pump-induced signal of triplet state along b-axis at low (170μJ/cm^2) and high (6600μJ/cm^2) pump influence. The pump beam was set at 795 nm. The polarization of the pump beam was set along b-axis of the hexacene single crystal. Related to Figure 3.

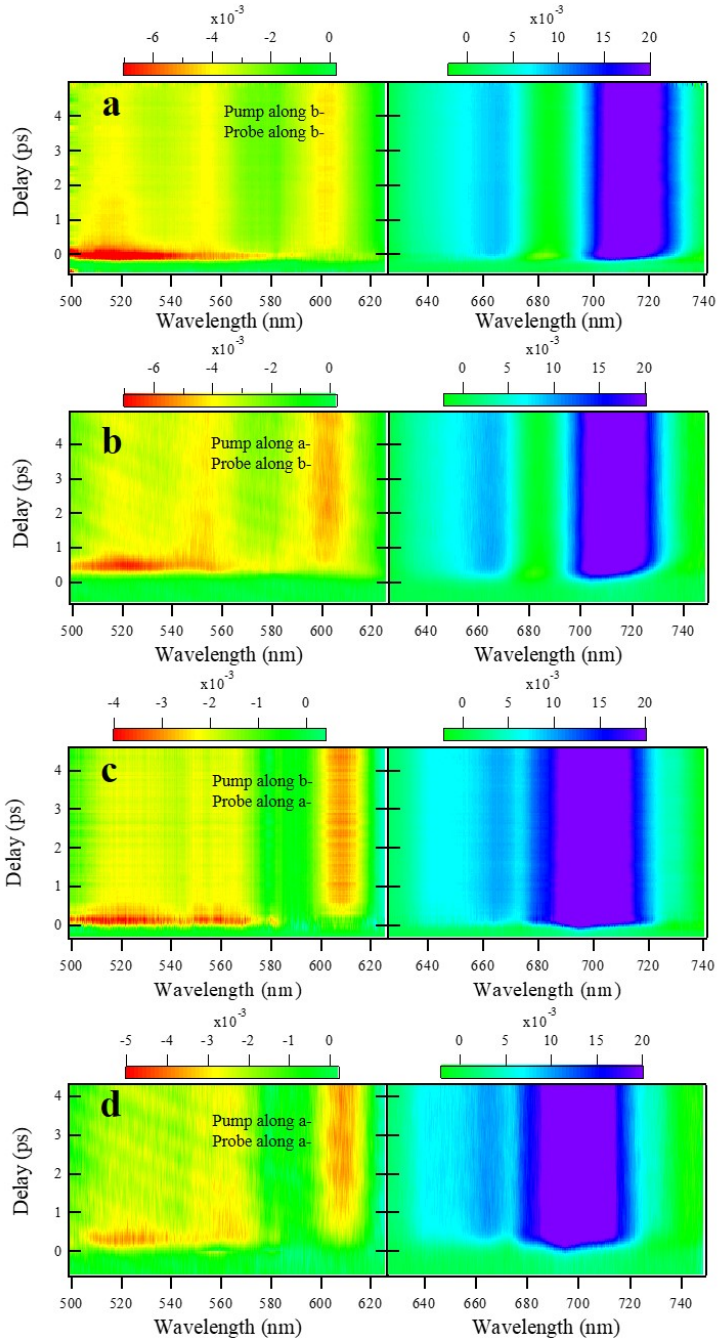

Figure S4 Comparison of transient spectra between all four possible polarization combinations: (a) ***b***-axis pump / ***b***-axis probe, (b) ***a***-axis pump / ***b***-axis probe, (c) ***b***-axis pump / ***a***-axis probe, (d) ***a***-axis pump / ***a***-axis probe. The transient responses of hexacene single crystals strongly depend on the probe polarization, whereas they are independent of the pump polarization. Related to Figure 3.

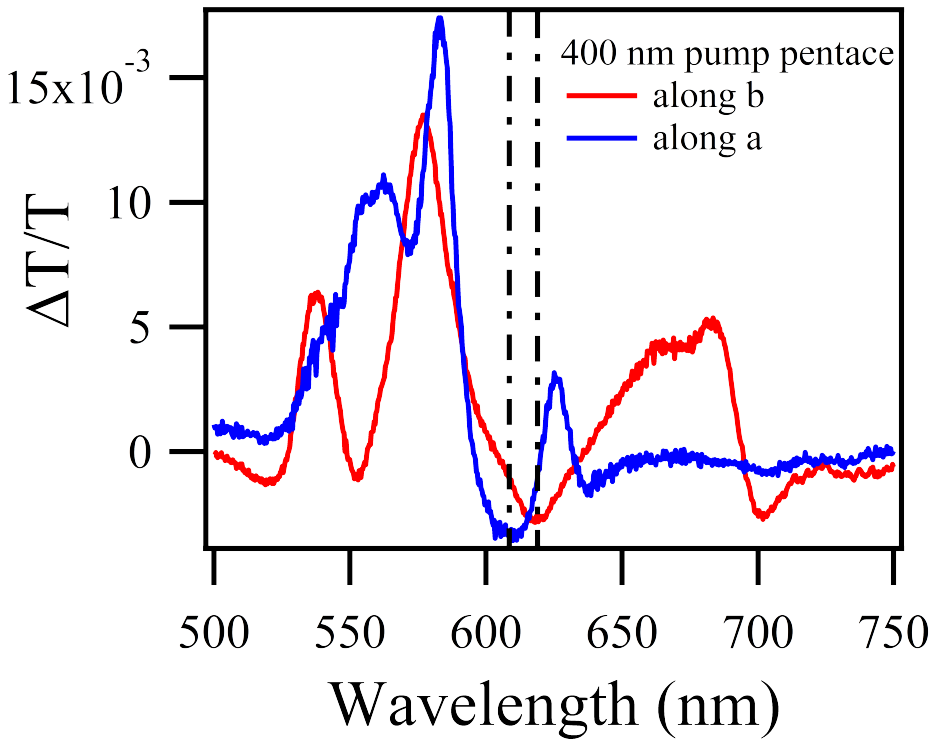

Figure S5. Transient absorption spectra of pentacene single crystals at a time delay of 4 ps probing along the long *a*- axis and short *b*-axis when a 400-nm photoexcitation is applied along the *b*-axis. The $T_1 \rightarrow T_n$ transitions exhibit different absorption peaks at 609 nm and 619 nm along the long *a*-axis and short *b*-axis, respectively. Related to Figure 3.

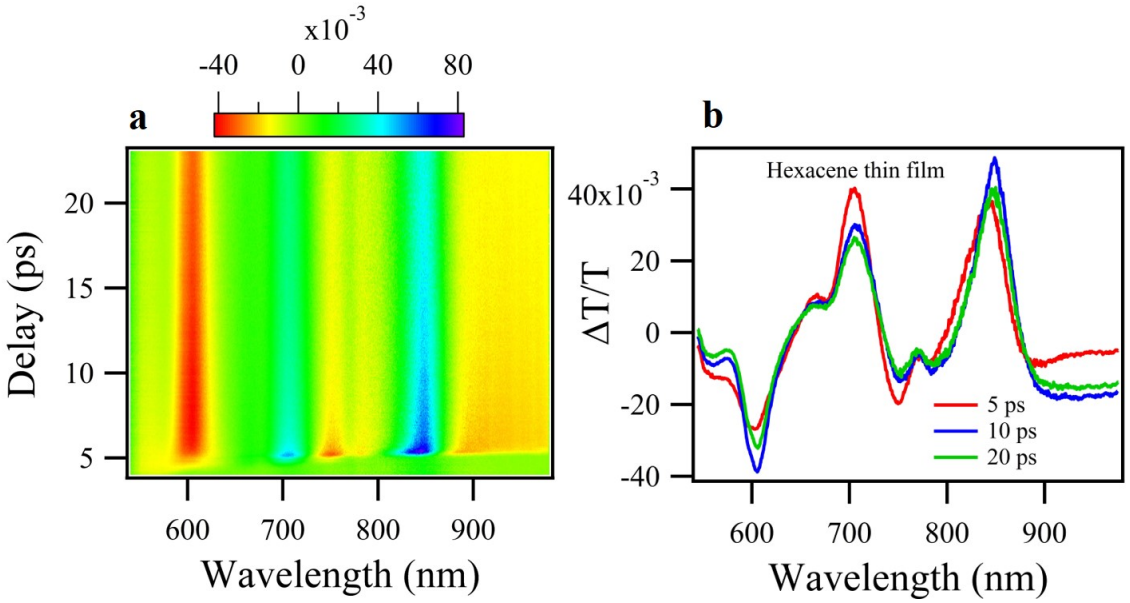

Figure S6. Singlet Fission in Hexacene Thin Film under 515 nm Photoexcitation. (a) Pseudo-color plots of transient absorption spectra from hexacene thin film excited at 515 nm. (b) Transient absorption spectra of hexacene thin film at times delay of 5, 10 and 15 ps. Related to Figure 3.

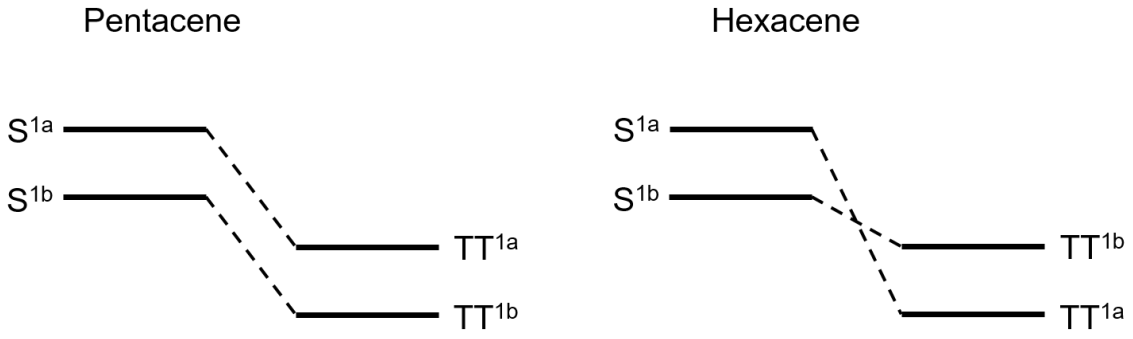

Figure S7 Energy diagram of singlet Davydov splitting and triplet Davydov splitting of pentacene and haxacene. Related to Figure 2.

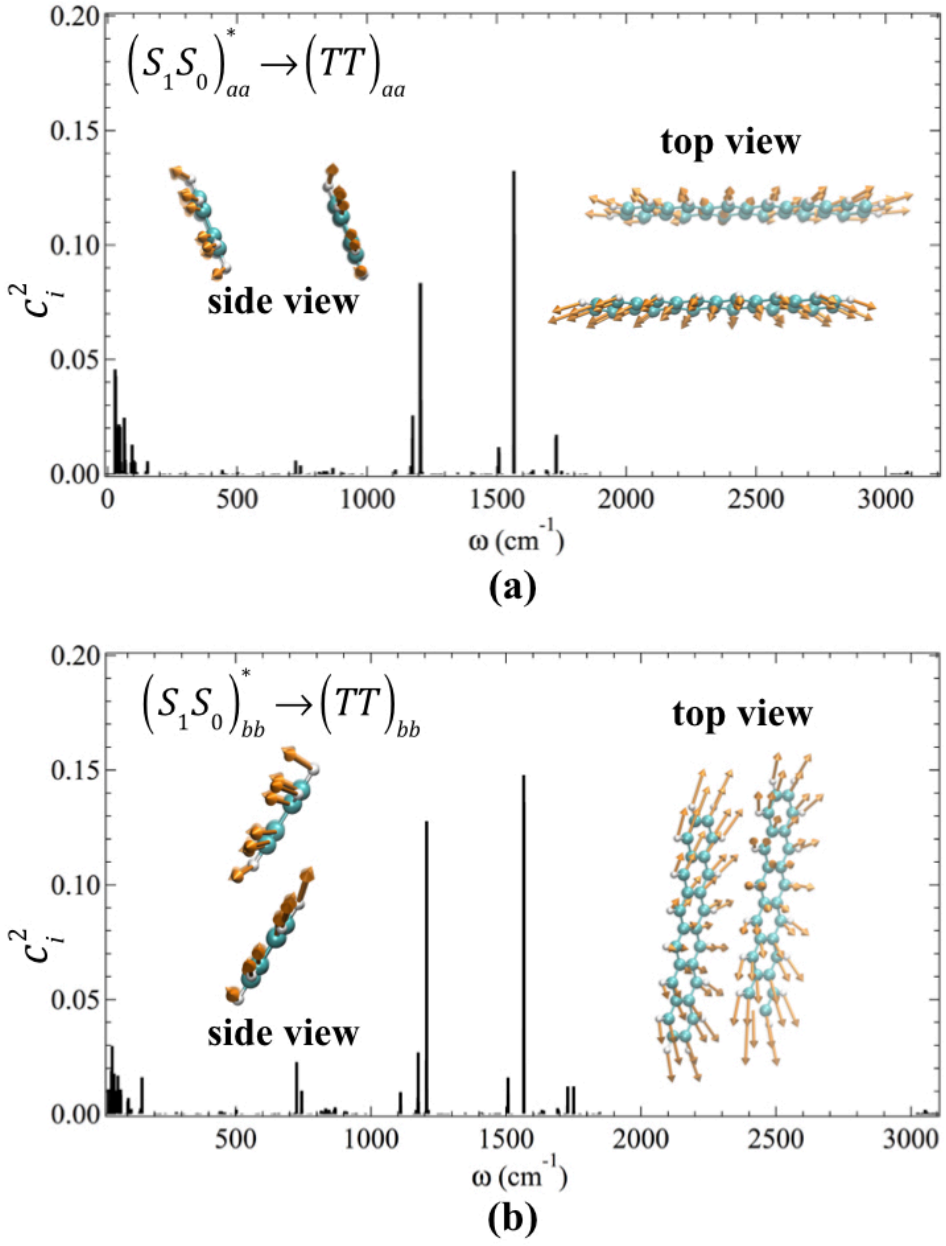

Figure S8. Calculated driving vibrational modes, $\vec{V}_{SF} = \sum_i c_i \vec{V}_i$, for singlet fission within an adjacent hexacene molecules along axes a and b. Their constituents in terms of c_i^2 are also presented alongside their side and top views. For visual clearance, only the displacement vectors on the participating molecules of singlet-fission are displayed. Related to Scheme 1.

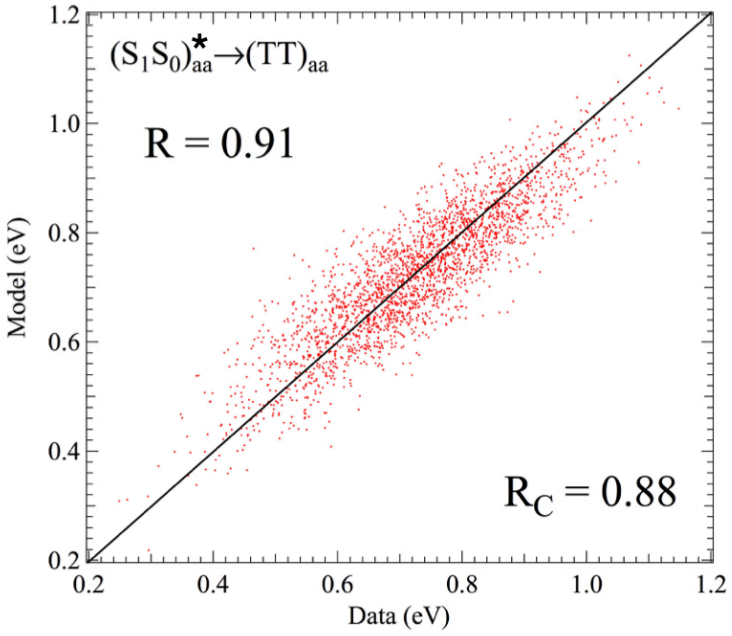

(a)

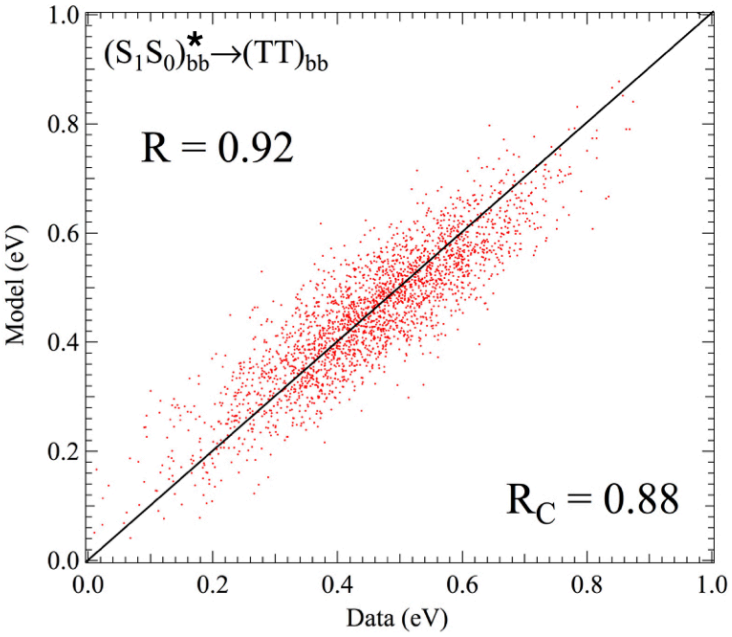

(b)

Figure S9. Scatter plots for the cross validation of $\vec{V}_{SF}$ along ***a*** and ***b*** axes. Related to Scheme 1.

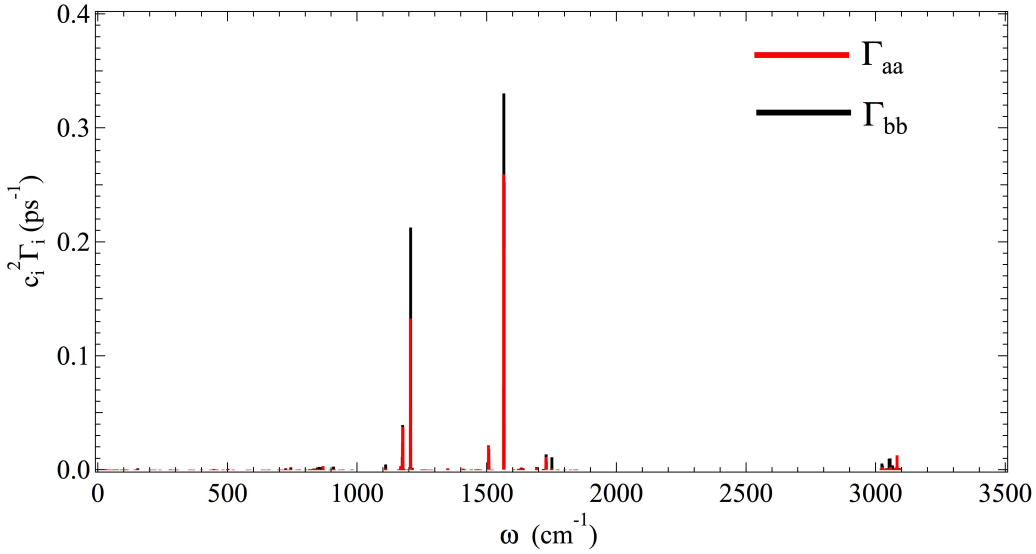

Figure S10. Profile of the thermal relaxation rate, Γ_i, of vibrational normal modes weighted by their relative importance, c_i^2, to the singlet-fission driving mode, $\vec{V}_{SF}$. Related to Scheme 1.

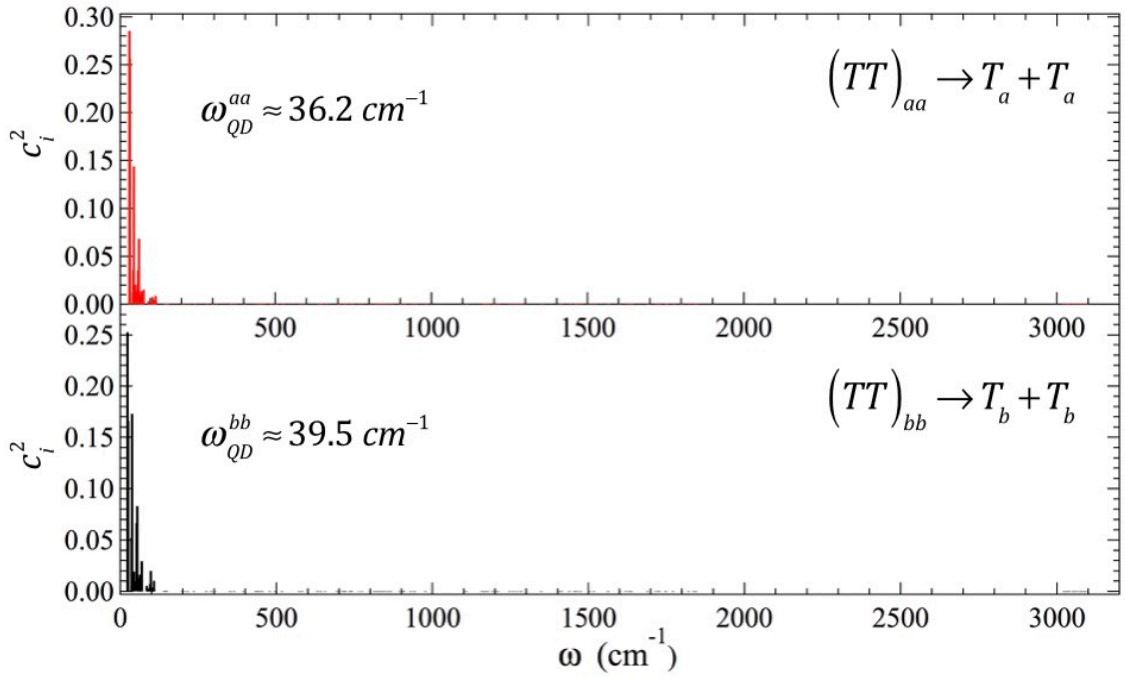

Figure S11. Components of the vibrational modes that drive quantum decoherence to decouple TT into $T+T$ along ***a*** and ***b*** axes. Related to Scheme 1.

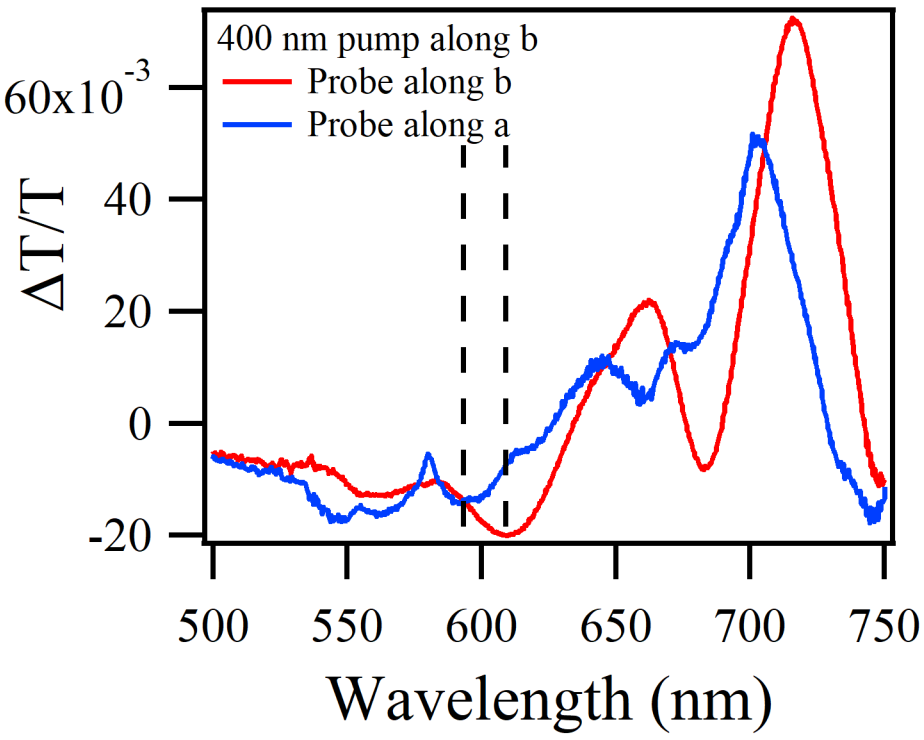

Figure S12. Transient absorption spectra of hexacene single crystals at a time delay of 6.4 ps probing along the long a- axis and short b-axis when a 400-nm photoexcitation is applied along the b-axis. The $T_1 \rightarrow T_n$ transitions exhibit different absorption peaks at 594 nm and 610 nm along the long a- axis and short b-axis, respectively. Related to Figure 3.

Supplemental Tables

Table S1. The energy gaps and oscillator strengths of the $S_0S_0 \rightarrow S_1S_0^*$ optical transitions along the ***a*** and ***b*** axes, alongside their projected transition dipole moments. Related to Figure 2.

lattice direction	aa	bb
$\Delta E\left(S_0S_0 \rightarrow S_1S_0^*\right)\left(eV\right)$	1.65	1.42
$f_{12}\left(10^{-3}\right)$	5.57	8.94
$D_a\left(debye\right)$	0.82	0.04
$D_b\left(debye\right)$	0.39	1.13
$D_c\left(debye\right)$	0.03	0.06

Table S2. Key parameters for the $S_0S_1 \rightarrow (TT)$ transition rate along axes a and b. ΔG_0 is the driving force, λ is the reorganization energy, J is the electronic coupling strength, Ω is the effective angular frequency of the driving vibrational mode, Γ is its thermal relaxation rate, k_F is the singlet fission rate, and k_D is the decay rate of S_0S_1. Related to Figure 4.

lattice direction	aa	bb
$\Delta G_0(eV)$	-0.62	-0.43
$\lambda(eV)$	0.46	0.40
$J(meV)$	9.2	10.9
$\Omega(cm^{-1})$	1752	1901
$\Gamma(ps^{-1})$	0.93	1.25
$k_F(ps^{-1})$	0.93	0.83
$k_D(ps^{-1})$	1.86	2.08

Table S3. Key parameters for the quantum decoherence rates, k_Q, along ***a*** and ***b*** axes according to the Redfield theory. Related to Figure 4 and Scheme 1.

lattice direction	aa	bb
$\Delta E_{QD}\ (meV)$	42	26
$\lambda\ (meV)$	8	6
$\omega_p\left(cm^{-1}\right)$	36.2	39.5
$k_Q\left(ps^{-1}\right)$	3.2	5.3

Transparent Methods

Preparation of Single Crystals

Hexacene single crystals were grown in a physical vapor transport (PVT) furnace at atmospheric pressure. Hexacene precursor was synthesized according to a previously reported method(Laudise et al., 1998; Watanabe et al., 2012). ~1 mg hexacene powder was heated in a hot zone of the furnace at 300 °C for a week. 50 SCCM of ultrahigh purity argon gas (99.999%) was used as purging gas as well as carrier gas. Hexacene single crystals were collected in the crystallization zone. Single crystals grown in this manner were first spread on a quartz substrate. The hexacene crystal face for this method tends to grow parallel to the substrate, namely (001). A gasket sealed container to hold the quartz substrate was assembled in the N_2 box to protect the single crystals from oxygen during optical experiments.

Experimental Setup for Micro Transmission UV-vis Spectrometer

The optical absorption measurements of hexacene single crystals were performed on a home-built microscope equipped with a lamp (Lumina-I) as an unpolarized broadband radiation source. Briefly, an intensity-tunable halogen-lamp and a LED pen light were used as the UV-vis light source for the UV-vis transmission measurements and the illumination light for the microscope, respectively. A beam splitter combined both the UV-vis and illumination light for a collinear light path. An objective with 10× magnification subsequently focused the selected polarized light onto a hexacene single crystal at normal incident angle. A condenser was used to collect the transmitted light that is turn was focused into a grating spectrometer (Andor Shamrock 500 with a grating blazed at 500nm, 150 groove/mm), followed by a thermo-cooled CCD (Andor Newton). A polarizer was placed between the lamp and the objective to select the polarization of the incident light. Only a few of crystallites met the requirements of the optical measurements on each substrate, even though small single crystals have been intentionally prepared. The thicknesses of the chosen hexacene samples were estimated to be on the order of ca. 0.5 μm according to the absorption coefficient of hexacene thin films reported in the literature. All experiments were performed at room temperature.

Micro-transient Absorption Spectrometer

A home-built microscope was coupled with a transient absorption setup for our micro-transient absorption measurements (Figure S1). We used 1 KHz regeneratively amplified Ti: Sapphire laser system to generate laser pulse with a center wavelength at 795 nm. The pulse duration is about 100 fs. The laser pulse was then split into two parts: one part was coupled with a motorized delay stage (Klinger) as a pump light, and the other part was focused onto a sapphire crystal plate to generate white light super-continuum as a probe light. Both the pump light and the probe light have been combined by a pellicle beam splitter and sent to the objective. Two more beam splitters were used along the beam path to couple the illumination light and a CMOS camera for imaging samples. The transmitted probe light was collected by a condenser and sent to the spectrometer and CCD (Andor Shamrock and Andor Newton, respectively). The pump light was blocked after passing the samples by placing an appropriate band pass filter. The time-dependent changes in absorption spectra have been obtained by switching on/off of the pump pulse. The CCD sampling rate of 200 Hz was synchronized with an optical chopper. A detection sensitivity of about 5×10^{-4} was achieved.

Estimation of Photo-excited Carrier Density for Singlet Fission

We estimated the photo-excited carrier density as follows:

1). We measured the transmission of the hexacene sample on quartz comparing with clean quartz substrate and observed approximately 20-fold decrease of the transmission light at 730 nm. By using a known extinction coefficient for hexacene single crystal at the same wavelength (0.25×10^5 cm^{-1}), we obtained the crystal thickness of about 520 nm.

$$I(z) = I(0) \cdot 10^{-\alpha(\lambda)z}$$
$$z = \log 20 / \alpha(\lambda) = 520\text{nm}$$

2). For 0.25 μW 795 nm femtosecond laser pulse, the number of photons per volume is given by

$$\frac{0.25\times10^{-6}}{10^{3}}\times\frac{3}{7}\times0.25\times10^{5}\,cm^{-1}\times0.52\times10^{4}\,cm\times$$
$$\frac{1}{\frac{1240}{795}\times1.6\times10^{-19}}\times\frac{1}{\pi\times(4.5\times10^{-4}\,cm)^{2}\times0.52\times10^{4}\,cm}$$
$$=2.1\times10^{19}\,cm^{-3}$$

3). If we assume that each absorbed photon generates one singlet exciton, the initial singlet exciton density is 2.1×10^{19} cm^{-3}.

4). Laser fluence:

$$\frac{Energy\,/\,pulse}{area}=\frac{0.25nJ/(7/3)}{\pi*(4.5\mu m)^{2}}=170\mu J/cm^{2}$$

5). Excitation volume:

$$\mathrm{V_{ext}}=\mathrm{Area}*\mathrm{Thickness}=\pi\cdot(4.5\mu\mathrm{m})^{2}\cdot0.52\mu\mathrm{m}=33\mu\mathrm{J/cm^{2}}$$

6). Volume of hexacene:

a=7.673Å, b=6.292Å, c=16.242Å

$$V=abc=784.13\ \mathrm{A}^{3}$$

Since there are two molecules in a unit cell, the volume of each molecule is 392.06 Å^3

7). The ratio of excited molecule density vs total molecule density:

$$\frac{\mathrm{D_{ext}}}{\mathrm{D_{tot}}}=\frac{2.1\times10^{19}\,\mathrm{cm^{-3}}}{1/392\mathrm{A}^{3}}=8.5\times10^{-3}$$

8). The expected pump probe signal without considering singlet fission:

$$\frac{\Delta\mathrm{T}}{\mathrm{T}}(\mathrm{S_0}-\mathrm{S_1})=\sigma(\mathrm{S_0})\times\mathrm{N}(\mathrm{S_1})=1.1\times10^{-2}$$

Coupled Rate Equations of Singlet Fission

$$S_0+S_1\xrightarrow{k_F}{}^{1}\left(T_1T_1\right)\xrightarrow{k_Q}T_1+T_1$$

k_F: the formation rate of a correlated triplet pair state

k_Q: the quantum decoherence rate of a correlated triplet pair state

By solving the two-step coupled rate equation, we can write the population dynamics for singlet and triplet exciton as

$$Singlet(\mathrm{t}) = \mathrm{A}_0\, e^{-k_F t}$$
$$TT(\mathrm{t}) = \frac{k_F\, \mathrm{A}_0}{k_F - k_Q}(e^{-k_F t} - e^{-k_Q t})$$
$$\mathrm{T}_1(\mathrm{t}) = \mathrm{A}_0(1 + \frac{1}{k_F - k_Q}(k_Q e^{-k_F t} - k_F e^{-k_Q t})) \qquad \text{Equation S1}$$

Global Fitting Based on Coupled Rate Equations for Singlet Fission

We noticed that all the kinetic traces include both the contributions from the $S_1 \rightarrow S_n$ and $T_1 \rightarrow T_n$ transitions. As such, we made our kinetic analyses by considering: 1) Transient responses at any energy are a sum of the $S_1 \rightarrow S_n$ and $T_1 \rightarrow T_n$ transitions; 2) Singlet fission is a two-step process with two independent rates, namely k_F and k_Q. The justification of the latter was based on the fact that the decay rate of S_1 is not consistent with the generation rate of T_1 from our kinetic data, in particular along the ***a*** axis. Specifically, we treat $\Delta T/T(E, t)$ as a sum of the contributions from both the S_1-S_n and T_1-T_n transitions at a given energy: $-\Delta T/T(E, t) = \sigma_{S1\text{-}Sn}(E) n_{S1}(t) + \sigma_{T1\text{-}Tn}(E) n_{T1}(t)$, where $n_{S1}(t)$ and $n_{T1}(t)$ are standard time-dependent populations of a two-step sequential reaction as given in Equation 1, and $\sigma_{S1\text{-}Sn}(E)$ and $\sigma_{T1\text{-}Tn}(E)$ are the cross sections for the $S_1 \rightarrow S_n$ and $T_1 \rightarrow T_n$ transitions.

Based on the kinetic model and the rate equations described above, we are able to apply the global fitting to our transient absorption data at different time delays. The change in measured transient transmission is proportional to the absorption cross section for each of the three following transitions: $S_0 \rightarrow S_1$, $S_1 \rightarrow S_n$ and $T_1 \rightarrow T_n$.

$$\begin{cases} \dfrac{\Delta T}{T}(S_1 - S_n) = -\sigma_S \times N_{S1}(t) \\ \dfrac{\Delta T}{T}(T_1 - T_n) = -\sigma_T \times N_{T1}(t) \\ \dfrac{\Delta T}{T}(S_0 - S_1) = \sigma_S \times (N_{S0}(0) - N_{S0}(t)) \\ N_{S0}(0) = N_{S0}(t) + N_{S1}(t) + N_{T1}(t) \end{cases}$$

Equation S2

Since the time-dependent spectra for the three transitions are highly overlapped, we treated every spectral region as a mixture of singlet and triplet excitons. Therefore, it takes the form as:

$$\frac{\Delta T}{T}(E,\ t) = (\sigma_{S0}(E,t) - \sigma_{S1}(E,t))N_{S1}(t) + (\sigma_{S0}(E,t) - \sigma_{T1}(E,t))N_{T1}(t)$$

In light of the excitation pulse temporal profile, we used the following fitting function for our data:

$$\frac{\Delta T}{T} = \frac{Erf(c1\times(t-c2))+1}{2} \times c3 \times e^{-k_F t} + c4 \times (1 + \frac{1}{k_F - k_Q}(k_Q e^{-k_F t} - k_F e^{-k_Q t}))$$

Equation S3

where Erf denotes the Gauss error function.

Triplet Davydov Splitting of Pentacene Single Crystals

We performed polarized transient absorption experiments on pentacene single crystals too. Figure S5 shows transient absorption spectra of pentacene single crystals at a time delay of 4 ps with probes along the long *a*-axis and the short *b*-axis when a 400-nm photoexcitation is applied along the *b*-axis. The $T_1 \rightarrow T_n$ transitions exhibit different absorption peaks at 608 nm and 618 nm along the long *a*- axis and short *b*-axis, respectively. The triplet Davydov splitting results show that the triplet energy level along the *b*-axis is higher than that along the *a*-axis, i.e., $E_{T_{1b}+T_{1b}} > E_{T_{1a}+T_{1a}}$.

Technical Details of Quantum Mechanics/Molecular Mechanics Simulations

In our hybrid quantum mechanics/molecular mechanics (QM/MM) study, density functional theory (DFT)(Hohenberg et al., 1964) was employed to accurately model the singlet fission process within a hexacene tetramer, which was selected to span along the ***a*** and ***b*** crystal axes. In addition, all nearest-neighboring molecules of the tetramer were also included in the QM subsystem to account for the electronic polarization effect. By contrast, generalized AMBER empirical force field (GAFF)(Wang et al., 2004) was used to efficiently describe the thermal fluctuation of other hexacene molecules consisting of the MM subsystem. Unless other specified, all QM/MM simulations were performed using CP2K package(VandeVondele et al., 2005) with Goedecker-Teter-Hutter (GTH) pseudopotential,(Goedecker et al., 1996) optimally tuned range-separated hybrid Perdew-Burke-Ernzerhof (ω-RSH-PBE) exchange-correlation functional,(Jacquemin et al., 2014) polarized-valence-double-ζ (PVDZ) basis set,(Woon et al., 1994) electrostatic QM/MM coupling scheme,(Laino et al., 2005) and a wavelet-based Poisson solver.(Genovese et al., 2006)

Simulated Formation Rate of Correlated Triplet Pair

As shown in Table S1, the optical gap for the $S_0S_0 \rightarrow S_0S_1^*$ transition along ***a*** axis is 1.65 eV, which is 0.23 eV higher than its counterpart along ***b*** axis. In spite of their relatively small difference on the optical gap, these two optical transitions have distinct oscillator strengths, i.e., 5.57×10^{-3} vs. 8.94×10^{-3}, making the light absorption along ***b*** axis nearly 60% stronger than that along ***a*** axis. Both of our calculated optical gaps and oscillator strengths are well in line with the experimental absorption spectrum (Figure. 1C).

In our FMSF theory(Elenewski et al., 2017b), the effective vibrational mode that drives singlet fission, is a linear combination of all normal modes, $\vec{V}_{SF} = \sum_i c_i \vec{V}_i$, where c_i reflects the relative importance of the i th normal mode. Mathematically, $\{c_i\}$ can be ascertained by maximizing the Pearson's correlation coefficient between $\{\vec{V}_i\}$ and $\{\Delta E_i^d\}$,(Chen, 2014) where $\Delta E^d = E_{S_0 S_1^*} - E_{TT}$ is the energy gap between $S_0 S_1^*$ and (TT). Specifically, our training set for $\vec{V}_{SF}$ consists of 3,000 snapshots extracted from a 3-ns trajectory of molecular dynamics (MD) simulation. As shown in Figure S8, regardless of the lattice direction of singlet fission, $\vec{V}_{SF}$ is always a ring-stretching mode that is collectively exerted by two adjacent hexacene molecules. Therefore, it is not surprising that the profile of c_i^2 features a few prominent peaks around 1200 cm^{-1} and 1500 cm^{-1}, making the vibrational quantum tunneling effect important for singlet fission since $\hbar\omega_{vib} \gg k_B T$. As a prudent measure to ensure the statistical quality of $\vec{V}_{SF}$, the determined c_i^2 were projected onto another 3000 snapshots extracted from a different MD trajectory for cross validation. It turns out that the cross-validated Pearson's coefficients, $R_C^{aa} = 0.88$ and $R_C^{bb} = 0.88$, are only slightly smaller than their counterparts of the training set $R^{aa} = 0.92$ and $R^{bb} = 0.91$ (Figure S9), suggesting satisfactory sampling for the functional mode analysis of $\vec{V}_{SF}$.

Once the composition of $\vec{V}_{SF}$ is ascertained, we can evaluate its effective angular frequency $\Omega = \sqrt{\frac{\lambda}{\hbar}\sum_{i=1} c_i^2 \omega_i}$ by assuming that the contribution of a given normal mode to

λ is proportional to its relative importance to $\vec{V}_{SF}$. As listed in Table S2, λ along ***a*** axis is 0.46 eV, which is 0.06 eV higher than that along ***b*** axis. The moderate difference on λ can be ascribed to a greater distortion of the hexacene crystal needed to accommodate a longer spin separation distance along ***a*** axis. Nevertheless, Ω_{aa} of 1752 cm^{-1} is even slightly slower than Ω_{bb} of 1902 cm^{-1} due to the higher weights of slower vibrational modes in $\vec{V}_{SF}$ along ***a*** axis (Figure S8). Interestingly, the values of both λ are less than $\left|\Delta G_0\right|$, placing the singlet fission into the inverted Marcus region. The applicability of Marcus-type non-adiabatic transition theory is further justified by our calculated feeble electronic coupling strengths of ~10 meV, which are in line with previous studies on other acenes.(Elenewski et al., 2017a; Yost et al., 2014)

Besides singlet fission, another important decay channel for an optically populated $S_0S_1^*$ vibronic state is its thermal relaxation. According to the phonon scattering theory,(Li et al., 2014) the lifetime of a given vibrational normal mode, $\vec{V}_i$, is decided by its anharmonic coupling with others. If only the third-order anharmonicity is considered, its decay rate, Γ_i is given by:

$$\Gamma_i = \sum_j \sum_k \frac{\hbar\pi\left(f_i + f_k + 1\right)}{4\omega_i\omega_j\omega_k}\left|\frac{\partial^3 E}{\partial\vec{V}_i\partial\vec{V}_j\partial\vec{V}_k}\right|^2 \delta\left(\omega_i - \omega_j - \omega_k\right) \qquad \text{Equation S4}$$

where ω s are the angular frequencies, $f = \frac{1}{e^{\hbar\omega/k_BT} - 1}$ is the Bose-Einstein distribution function, $\frac{\partial^3 E}{\partial\vec{V}_i\partial\vec{V}_j\partial\vec{V}_k}$ is the third-order derivate of energy with respect to all participating

normal modes, and δ is the Dirac delta function. Using the ALAMODE simulation package,(Tadano et al., 2014) the third-order anharmonicity of our system was evaluated through a non-linear least squares regression subject to translational symmetry constraint. Thereafter, Γ_i was calculated by exploring all energy-conversing scattering events. The profile of Γ_i weighted by c_i^2 (Figure S10) again features a couple of distinct peaks at ~1200 cm^{-1} and ~1500 cm^{-1}, further signifying the importance of these ring-stretching normal modes not only to singlet fission but also to thermal relaxation. Now, with all needed parameters in hand, we can apply Eq.2 to calculate k_F under non-thermalized condition. It was found that k_F^{aa} of 0.93 ps^{-1} is nearly same as k_F^{bb} of 0.83 ps^{-1}, in spite of a modest disparity in energetic parameters such as ΔG_0 and λ. The diminished difference on k_F along ***a*** and ***b*** axes primarily arises from their fast Ωs, whose zero-point energies become much more overwhelming for vibrational quantum tunneling. If the fluorescent decay of $S_0S_1^*$ to S_0S_0 is negligible, the overall decay rate, k_D, of $S_0S_1^*$ is simply $k_F + \Gamma$, leading to k_D^{aa} of 1.86 ps^{-1} and k_D^{bb} of 2.08 ps^{-1}.

Derivation of Energy Gap Associated with Quantum Decoherence

Using a two-electron-two-orbital scheme, one can easily construct the three constituent states for a molecule at its triplet state:

$$T_x = \left\{ \begin{array}{c} \left(\begin{array}{c} \uparrow \\ \uparrow \end{array} \right) \begin{array}{l} a \\ b \end{array} \\ \frac{1}{\sqrt{2}} \left(\begin{array}{c} \downarrow \\ \uparrow \end{array} + \begin{array}{c} \uparrow \\ \downarrow \end{array} \right) \\ \left(\begin{array}{c} \downarrow \\ \downarrow \end{array} \right) \end{array} \right. \qquad \text{Equation S5}$$

where we denote the upper and lower orbitals as a and b, respectively. Similarly, we can construct another molecule's triplet state using different upper and lower orbitals denoted as c and d:

$$\left. \begin{array}{c} \begin{array}{l} c \\ d \end{array} \left(\begin{array}{c} \uparrow \\ \uparrow \end{array} \right) \\ \frac{1}{\sqrt{2}} \left(\begin{array}{c} \downarrow \\ \uparrow \end{array} + \begin{array}{c} \uparrow \\ \downarrow \end{array} \right) \\ \left(\begin{array}{c} \downarrow \\ \downarrow \end{array} \right) \end{array} \right\} = T_y \qquad \text{Equation S6}$$

For a fully decoupled $T_x + T_y$ dimer, all nine possible cross-molecule combinations of the constituent states are equally weighted, resulting in an energy expectation value of

$$E_{T_x+T_y} = -k_b T \ln(3\times 3) + E_{coulomb} + E_x^{ab} + E_x^{cd} + \frac{1}{2}\left(E_x^{ac} + E_x^{bc} + E_x^{ad} + E_x^{bd}\right) \qquad \text{Equation S7}$$

where $k_b \ln(3\times 3)$ is the electronic entropy, T is the temperature, $E_{coulomb}$ is the coulomb energy arising from all orbital pairs, and E_x stands form the exchange energy between a selected orbital pair. For example, E_x^{ab} is the exchange energy between orbital a and orbital b.

Alternatively, $E_{T_x+T_y}$ can be expressed as

$$E_{T_x+T_y} = -k_b T \ln 9 + \frac{3}{2} E_{HS} - \frac{1}{2} E_{LS}$$

Equation S8

where E_{HS} and E_{LS} are the energies of the following spin configurations:

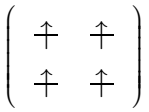 and 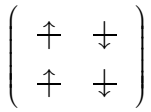 , respectively.

For a $\left(T_x T_y\right)$ pair at its singlet state:

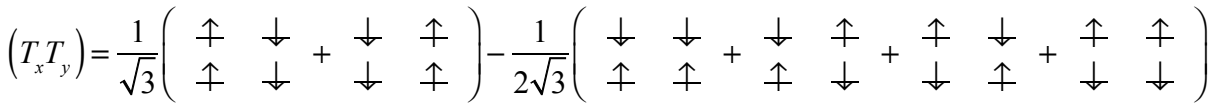

Equation S9

its energy is given by:

$$E_{\left(T_x T_y\right)} = k_b T \ln\left(9\right) + E_{coulomb} + E_x^{ab} + E_x^{cd} - \frac{1}{2}\left(E_x^{ac} + E_x^{bc} + E_x^{ad} + E_x^{bd}\right)$$

Equation S10

which can be further simplified as

$$E_{\left(T_x T_y\right)} = \frac{1}{2} E_{HS} + \frac{1}{2} E_{LS}$$

Equation S11

Through a comparison between Eq. 4 and Eq. 7, we found that

$$\Delta E_{QD} = E_{\left(T_x T_y\right)} - E_{T_x+T_y} = k_b T \ln 9 + E_{LS} - E_{HS} = k_b T \ln 9 + E_{HS \to LS}$$

Equation S12

where $E_{HS\rightarrow LS}$ is the associated spin-flip energy.

Reference

Chen, H., (2014). Functional Mode Electron-Transfer Theory. J. Phys. Chem. C *118*, 7586-7593.

Elenewski, J.E., Cubeta, U.S., Ko, E., Chen, H., (2017a). Computer Simulation of Singlet Fission in Single Crystalline Pentacene by Functional Mode Vibronic Theory. J. Phys. Chem. C *121*, 11159-11165.

Elenewski, J.E., Cubeta, U.S., Ko, E., Chen, H., (2017b). Functional Mode Singlet Fission Theory. J. Phys. Chem. C *121*, 4130-4138.

Genovese, L., Deutsch, T., Neelov, A., Goedecker, S., Beylkin, G., (2006). Efficient solution of Poisson's equation with free boundary conditions. J. Chem. Phys. *125*, 074105.

Goedecker, S., Teter, M., Hutter, J., (1996). Separable dual-space Gaussian pseudopotentials. Phys. Rev. B *54*, 1703-1710.

Hohenberg, P., Kohn, W., (1964). Inhomogeneous Electron Gas. Phys. Rev. *136*, B864-B871.

Jacquemin, D., Moore, B., Planchat, A., Adamo, C., Autschbach, J., (2014). Performance of an Optimally Tuned Range-Separated Hybrid Functional for 0–0 Electronic Excitation Energies. J. Chem. Theory Comput. *10*, 1677-1685.

Laino, T., Mohamed, F., Laio, A., Parrinello, M., (2005). An Efficient Real Space Multigrid QM/MM Electrostatic Coupling. J. Chem. Theory Comput. *1*, 1176-1184.

Laudise, R.A., Kloc, C., Simpkins, P.G., Siegrist, T., (1998). Physical vapor growth of organic semiconductors. J. Cryst. Growth *187*, 449-454.

Li, W., Carrete, J., A. Katcho, N., Mingo, N., (2014). ShengBTE: A solver of the Boltzmann transport equation for phonons. Comput. Phys. Commun. *185*, 1747-1758.

Tadano, T., Gohda, Y., Tsuneyuki, S., (2014). Anharmonic force constants extracted from first-principles molecular dynamics: applications to heat transfer simulations. J. Phys.: Condens. Matter *26*, 225402.

VandeVondele, J., Krack, M., Mohamed, F., Parrinello, M., Chassaing, T., Hutter, J., (2005). Quickstep: Fast and accurate density functional calculations using a mixed Gaussian and plane waves approach. Comput. Phys. Commun. *167*, 103-128.

Wang, J., Wolf, R.M., Caldwell, J.W., Kollman, P.A., Case, D.A., (2004). Development and testing of a general amber force field. J. Comput. Chem. *25*, 1157-1174.

Watanabe, M., Chang, Y.J., Liu, S.-W., Chao, T.-H., Goto, K., Islam, M.M., Yuan, C.-H., Tao, Y.-T. *et. al.*, (2012). The synthesis, crystal structure and charge-transport properties of hexacene. Nat. Chem. *4*, 574-578.

Woon, D.E., Jr., T.H.D., (1994). Gaussian basis sets for use in correlated molecular calculations. IV. Calculation of static electrical response properties. J. Chem. Phys. *100*, 2975-2988.

Yost, S.R., Lee, J., Wilson, M.W.B., Wu, T., McMahon, D.P., Parkhurst, R.R., Thompson, N.J., Congreve, D.N. *et. al.*, (2014). A transferable model for singlet-fission kinetics. Nat. Chem. *6*, 492-497.